
1 Atmospheric mercury speciation dynamics at the high-altitude Pic du Midi
2 Observatory, southern France

3
4 X. W. Fu^{1,2}, N. Maruszczak¹, L.-E. Heimbürger^{1,3}, B. Sauvage⁴, F. Gheusi⁴, E. M.
5 Prestbo⁵, J. E. Sonke¹,

6 ¹Observatoire Midi-Pyrénées, Laboratoire Géosciences Environnement Toulouse, CNRS/IRD/Université de
7 Toulouse, 14, avenue Édouard Belin, 31400 Toulouse, France

8 ²State Key Laboratory of Environmental Geochemistry, Institute of Geochemistry, Chinese Academy of Sciences,
9 Guiyang, China.

10 ³Mediterranean Institute of Oceanography, Campus de Luminy, 13288 Marseille, France

11 ⁴Observatoire Midi-Pyrénées, Laboratoire d'Aérologie, CNRS/IRD/Université de Toulouse, 14, avenue Édouard
12 Belin, 31400 Toulouse, France

13 ⁵Tekran Research and Development, 330 Nantucket Blvd., Toronto, ON, Canada M1P2P4

14 Correspondence to: Xuewu Fu (foxuewu@mail.gyig.ac.cn)
15

16 Abstract: Continuous measurements of atmospheric gaseous elemental mercury (GEM),
17 particulate bound mercury (PBM) and gaseous oxidized mercury (GOM) at the high-altitude Pic
18 du Midi Observatory (PDM Observatory, 2877 m a.s.l) in southern France were made from Nov
19 2011 to Nov 2012. The mean GEM, PBM and GOM concentrations were 1.86 ng m^{-3} , 14 pg m^{-3}
20 and 27 pg m^{-3} , respectively and we observed 44 high PBM (peak PBM values of 33- 98 pg m^{-3})
21 and 61 high GOM (peak GOM values of 91-295 pg m^{-3}) events. The high PBM events occurred
22 mainly in cold seasons (winter and spring) whereas high GOM events were mainly observed in the
23 warm seasons (summer and autumn). In cold seasons the maximum air mass residence times
24 (ARTs) associated with high PBM events were observed in the upper troposphere over North
25 America. The ratios of high PBM ARTs to total ARTs over North America, Europe, the Arctic
26 region and Atlantic Ocean were all elevated in the cold season compared to the warm season,
27 indicating that the middle and upper free troposphere of the Northern Hemisphere may be more
28 enriched in PBM in cold seasons. PBM concentrations and PBM/GOM ratios during the high
29 PBM events were significantly anti-correlated with atmospheric aerosol concentrations, air
30 temperature and solar radiation, suggesting in situ formation of PBM in the middle and upper
31 troposphere. We identified two distinct types of high GOM events with the GOM concentrations
32 positively and negatively correlated with atmospheric ozone concentrations, respectively. High
33 GOM events positively correlated with ozone were mainly related to air masses from the upper
34 troposphere over the Arctic region and middle troposphere over the temperate North Atlantic
35 Ocean, whereas high GOM events anti-correlated with ozone were mainly related to air masses
36 from the lower free troposphere over the subtropical North Atlantic Ocean. The ARTs analysis
37 demonstrates that the lower and middle free troposphere over the North Atlantic Ocean was the
38 largest source region of atmospheric GOM at the PDM Observatory. The ratios of high GOM
39 ARTs to total ARTs over the subtropical North Atlantic Ocean in summer were significantly higher
40 than those over the temperate and sub-arctic North Atlantic Ocean as well as that over the North
41 Atlantic Ocean in other seasons, indicating abundant in situ oxidation of GEM to GOM in the
42 lower free troposphere over the subtropical North Atlantic Ocean in summer.
43

44 1 Introduction

45 Transformations of mercury (Hg) in the atmosphere play a crucial role in the global Hg cycle
46 (Selin et al., 2007; Driscoll et al., 2013). Gaseous elemental mercury (GEM) is the predominant
47 form emitted by anthropogenic and natural sources (Pirrone et al., 2010). GEM is then
48 transformed to gaseous oxidized mercury (GOM) and particulate bound mercury (PBM) by
49 oxidation. Atmospheric Hg deposition occurs by wet deposition and dry deposition pathways.
50 Models suggest global GEM dry deposition to be potentially important, yet lack broad
51 observational evidence (Selin et al., 2008). On the other hand, GOM and PBM are readily
52 scavenged from the atmosphere by **wet deposition and dry deposition pathways. Due to its fast dry**
53 **deposition velocities, GOM is thought to be mainly scavenged from the atmosphere by dry**
54 **deposition, whereas wet deposition plays a more important role in the removal of PBM in the**
55 **atmosphere** (Lee et al., 2001; Zhang et al., 2009; Lin et al., 2010). Hence, conversion of GEM to
56 GOM and PBM is a crucial process in the removal of Hg in the atmosphere, which in turn affects
57 the loading of Hg to terrestrial and marine ecosystems.

58 Conversion of GEM to GOM and PBM is potentially occurring throughout the global
59 atmosphere, but the rates of conversion are thought to vary and are dependent on the levels of
60 atmospheric oxidants and environmental factors. Current modeling studies suggested that
61 conversion of GEM to GOM and PBM produces approximate 8000 tons of GOM and PBM
62 annually, which explains at least 90% of the total sources of GOM and PBM in the atmosphere
63 (Holmes et al., 2010). However, it is still unclear where the majority of the conversion takes place,
64 by what mechanism and **which** major oxidants and environmental factors are involved. Over the
65 last decade, studies have been carried out to measure atmospheric Hg speciation at high-altitude
66 sites in the USA and Asia and on research flights. A study at the Mount Bachelor observatory
67 (MBO, USA) showed elevated GOM (up to 600 pg m⁻³) and low GEM in the free troposphere,
68 suggesting in situ oxidation (Swartzendruber et al., 2006). Observations at Storm Peak laboratory
69 (SPL, USA) and Lulin Atmospheric Background Station (LABS, Taiwan) showed similar, though
70 less elevated, GOM events in free tropospheric air masses (Fain et al., 2009; Sheu et al., 2010).
71 Long-term Hg speciation observations at MBO suggest GEM oxidation to be enhanced in
72 long-range Asian pollution plumes, but also in marine boundary layer (MBL) air masses
73 originating over the Pacific Ocean (Timonen et al., 2013). INTEX-B in-flight observations of
74 GEM in the tropopause region (8-12km) have shown low GEM levels, sometimes down to zero,
75 indicative of rapid oxidation (Talbot et al., 2007). CARIBIC in-flight observations of total gaseous
76 Hg (TGM ~ GEM+GOM) showed lower TGM levels in the southern hemisphere, TGM depletion
77 in the extratropical lowermost stratosphere and a general **negative** correlation between TGM and
78 ozone (Slemr et al., 2009; Slemr et al., 2014). In-flight, in-situ analyses of stratospheric aerosols

79 suggest that the upper troposphere and lower stratosphere depletion in GEM is balanced by
80 abundant PBM (Murphy et al., 1998;Murphy et al., 2006). Recent in-flight measurements
81 provided the first simultaneous observations of both GEM and the combined GOM+PBM
82 fractions at an altitude above 6 km (Lyman and Jaffe, 2012). The study showed elevated
83 GOM+PBM levels in stratospheric air masses and confirmed the importance of stratospheric
84 GEM oxidation. The findings of all these studies indicate that the free troposphere and lower
85 stratosphere are important regions for conversion of GEM to GOM and PBM.

86 A recent study reviewed mountain-top studies of free troposphere Hg dynamics and
87 compared observations to the GEOS-Chem atmospheric Hg chemistry and transport
88 model(Weiss-Penzias et al., 2015). The model intercompared Hg oxidation by Br against
89 OH-ozone pathways and was able to only marginally reproduce observations, indicating the need
90 to improve both measurement techniques and models. Additional long-term observations of GEM,
91 GOM, and PBM are therefore necessary to map out regions and altitudes that favor GEM
92 oxidation, and provide insight into the oxidation mechanisms. In the present study, we carried out
93 one year of continuous measurements of speciated atmospheric mercury at the Pic du Midi (PDM)
94 Observatory, a high-altitude site (2877 m a.s.l) in the French Pyrenees mountains. This is the first
95 year-around study of atmospheric Hg speciation at a mid-latitude high-altitude site. This study
96 may help to better understand the seasonal patterns of high GOM and PBM events and the
97 mechanisms underlying the transformations of atmospheric Hg in the free troposphere over the
98 lower, middle and high latitudes.

100 **2 Materials and methods**

101 **2.1 Site description**

102 The Pic du Midi (PDM) Observatory (0.142° E, 42.937° N, 2877 m a.s.l) is a high-altitude
103 monitoring station situated on top of an isolated peak (elevated approximately 1300 m relative to
104 the surrounding terrain) on the northern edge of the central Pyrenees mountains, Southwest France.
105 It is approximately 150 km to the east of the North Atlantic coast and 210 km to west of the
106 Mediterranean Sea. The PDM Observatory frequently receives free tropospheric air from the
107 North Atlantic and Europe (Henne et al., 2010). The station may also be partly influenced by
108 boundary layer air transported by plain-to-mountain winds from southwest France or through
109 regional transport from Spain under southerly or south-westerly synoptic wind conditions(Gheusi
110 et al., 2011;Tsamalis et al., 2014). There are no point **sources** around the station or in the
111 surrounding areas. The two nearest cities are Pau and Tarbes which are respectively located 60 and
112 30 km northwest to the station and may influence the observations via upslope transport.

113

114 2.2 Measurements of speciated atmospheric mercury and Ancillary parameters

115 Speciated atmospheric Hg is continuously measured at the PDM Observatory using the
116 Tekran 2537/1130/1135 system (Tekran Inc., Canada). The period analyzed in this study goes from
117 18th Nov 2011 to 17th Nov 2012. The Tekran system has been widely used and described in detail
118 elsewhere (Landis et al., 2002; Lindberg et al., 2002). Briefly, GOM, PBM, and GEM in ambient
119 air were collected onto KCl-coated annular denuder, regenerable quartz fiber filter and dual gold
120 cartridges in sequence. The system was programmed to collect GOM and PBM at 1-h intervals at
121 a volumetric flow rate of 10 L min⁻¹; and GEM was collected at 5-min intervals at a volumetric
122 flow rate of 1.07 L min⁻¹. Once collected, Hg is thermally decomposed from each unit and
123 detected by cold vapor atomic fluorescence spectroscopy (CVAFS) as Hg⁰. **GEM concentrations**
124 **were directly measured by the Tekran 2537 Analyzer. Recent studies have suggested that the**
125 **biased integration of small mercury loads (e.g. <~10 pg) may lead to a low bias of GOM and PBM**
126 **concentrations (Slemr et al., 2016; Swartzendruber et al., 2009). In this study, final GOM and PBM**
127 **concentrations were calculated following the method proposed by the Atmospheric Mercury**
128 **Network (AMNet) quality control (Steffen et al., 2012). Concentrations of GEM are expressed in**
129 **ng m⁻³ (STP) and GOM and PBM are expressed in pg m⁻³ (STP) with standard temperature of**
130 **273.14 K and pressure of 1013 hPa.** KCl-coated denuder, Teflon coated glass inlet, and impactor
131 plate were replaced bi-weekly and quartz filters were replaced monthly. Denuders and quartz
132 filters were prepared and cleaned before field sampling following the methods in Tekran technical
133 notes. The Tekran 2537B analyzer was routinely calibrated using its internal permeation source at
134 a 47 h interval, and was also cross-calibrated every 3 months against an external temperature
135 controlled Hg vapor standard. Due to the frequent extreme weather conditions at the PDM
136 Observatory, the system was installed inside a temperature-controlled laboratory. Ambient air was
137 introduced into the Tekran unit using the Tekran 1004 Teflon coated manifold, which is similar as
138 that used at the MBO, USA (Swartzendruber et al., 2006). The inlet of the Tekran 1104 manifold
139 was about 0.5 m from the outside wall of the laboratory and oriented to the southwest (the local
140 predominant wind direction) of the laboratory. Temperature of the Tekran 1104 manifold was kept
141 at 70 °C and air flow through the manifold was about 100 L min⁻¹. Blanks of Tekran unit and
142 manifold were quantified at the beginning and end of each maintenance (bi-weekly) using Hg-free
143 ambient air. The annual mean GEM blank of the Tekran unit was 0.04 ± 0.03 ng m⁻³ (1SD) and
144 detection limit of GEM was estimated to be 0.1 ng m⁻³.

145 Measurement of GOM and PBM is challenging due to the typical low part per quadrillion
146 (ppq) concentrations, reactivity and potential for species interconversion, and the need to
147 pre-concentrate on a surface. In addition the lack of understanding of the specific forms and
148 accepted calibration standards of GOM and PBM hinders the ability to obtain in-field quality

149 assurance measurements, like dynamic spiking under changing atmospheric conditions. Recently,
150 uncertainties regarding the accuracy of GOM measurements have been discovered related to O₃
151 and water vapor levels suggesting a potential for low GOM bias under certain atmospheric
152 conditions (Lyman et al., 2010;Gustin et al., 2013). Another study suggested that **GOM**
153 **concentrations measured by cation exchange membranes were 1.3 to 3.7 times higher than that**
154 **measured by KCl-coated denuders**, but was only a comparison of two differing methods, with
155 neither one challenged in real time by standard spiking under atmospheric conditions (Huang et al.,
156 2013). On the other hand, the potential for the PBM to be biased has not been thoroughly studied
157 and understood, for the reasons mentioned above, however the bias would likely be positive due to
158 GEM uptake as the regenerable filter ages and becomes more reactive. At **the** PDM Observatory,
159 similar to other high altitude studies, we do not observe simultaneous increases of PBM during
160 high GOM events suggesting no significant GOM breakthrough or GEM uptake on the filter
161 (Malcolm and Keeler, 2007;Swartzendruber et al., 2006;Fain et al., 2009). Similarly GOM loss
162 from denuders has been suggested to relate to high humidity levels (McClure et al., 2014). The
163 elevated free tropospheric PBM and GOM events discussed in this study occur predominantly in
164 low humidity air masses (median humidity of 21 and 28 % respectively) limiting GOM losses.
165 Therefore, as most of the discussion in the present study is based on the relative variations of
166 GOM and PBM, we assume the potential sampling artifacts may bring a minimal uncertainty to
167 the overall findings. Most importantly, the method used in this study and others is “state of the art”
168 at this time and has resulted in profound discoveries that are scientifically coherent (Schroeder and
169 Munthe, 1998;Laurier et al., 2003;Lindberg et al., 2002;Swartzendruber et al., 2006;Steffen et al.,
170 2008;Sprovieri et al., 2010;Fu et al., 2015). Currently, there is no better method to routinely
171 separate and quantify low, part-per-quadrillion concentrations of the mercury fractions with hourly
172 time resolution, than the use of a fully heated sample train that rejects large particles (>2.5 μm) by
173 impaction, capture of “sticky” GOM species on a laminar flow, coated annular denuder, which
174 rejects both PBM and GEM, followed by a quartz fiber filter to collect PBM, which rejects GEM
175 so it can pass to a sensitive monitor for continuous detection. The operationally defined method to
176 quantify atmospheric mercury fractions is similar to well established methods used for other
177 “sticky gases” ammonia and nitric acid.

178 Atmospheric CO and ozone concentrations were continuously measured using the TEI
179 48CTL gas filter correlation analyzers and 49C Ozone analyzer (Thermo Environmental
180 Instruments Inc. USA), respectively. Detailed information regarding the principle of the
181 instruments, calibrations, and measurement uncertainties can be found in a previous study (Gheusi
182 et al., 2011).The standard uncertainties associated with CO and ozone datasets (15-min averaged
183 data) were reported to be 6.6 and 1.2 ppbv, respectively (Gheusi et al., 2011). Atmospheric aerosol

184 number concentration in PM₁₀ particles (i.e. of diameter < 10 μm) was measured at the PDM
185 Observatory using a condensation particle counter (CPC), Model 3010 by TSI Inc. The particles
186 are detected by condensing butanol vapor onto the particles, causing them to grow into droplets.
187 These particles (in the droplet form) are then counted by optical absorption (Gheusi et al., 2011).
188 CO and ozone mole fractions, as well as atmospheric aerosol number concentration and standard
189 meteorological variables at the PDM Observatory were obtained as 5-min averages from the PAES
190 (French acronym for atmospheric pollution at synoptic scale; <http://paes.aero.obs-mip.fr/>)
191 network.

192

193 **2.3 Simulations of back trajectories, air masses residence times and potential source regions**

194 In the present study, we calculated 10-day back normal trajectory for high PBM events and
195 7-day back normal trajectory for high GOM events, respectively using the NOAA Hysplit
196 trajectory model and gridded meteorological data (Global Data Assimilation System, GDAS1)
197 (Draxler and Rolph), which are close to the upper range of the lifetime of GOM and PBM in the
198 atmosphere (Schroeder and Munthe, 1998; Driscoll et al., 2013). The GDAS1 has a horizontal
199 resolution of 1 degree (360×180 grid cells) with 23 vertical levels from 1000 hPa to 20 hPa. The
200 trajectories ended at the PDM Observatory at a height of 3000 m a.s.l. (approximately 100 m
201 above the sampling site). In addition, we also used the Flexpart Lagrangian particle dispersion
202 model version 9.0 (Stohl et al., 2005) to simulate the 20 days back trajectories for two special
203 events (high PBM event #12 and #19) and to make a comparison with Hysplit. The Flexpart
204 model is driven by wind fields provided by the European Centre for Medium-range Weather
205 Forecast (ECMWF) with a temporal resolution of 3 hours (analyses at 00:00, 06:00, 12:00, 18:00
206 UTC; forecasts at 03:00, 09:00, 15:00, 21:00 UTC) and with horizontal resolution of 32 km. The
207 model output refers to the time, in seconds, the released particles spent in each output grid box
208 before reaching the PDM Observatory. Flexpart residence times are output every 3 h on a uniform
209 grid of 0.5° latitude × 0.5° longitude in 40 vertical layers from mean sea level to a height of 20 km
210 above sea level. In the present study, we analyzed how air masses from different sublayers in the
211 troposphere affect atmospheric PBM and GOM concentrations at the PDM Observatory. We
212 subdivide the troposphere into 4 sublayers: boundary layer (> 900 hPa), lower free troposphere
213 (700-900 hPa), middle free troposphere (500-700 hPa) and upper free troposphere (200-500 hPa).

214 Air mass residence times (ARTs) were calculated on the basis of the simulations of 7-day
215 backward trajectories ending at the PDM Observatory. The studied domain covered by the
216 trajectories was divided into 3590 grid cells of 2.5° latitude × 2.5° longitude. To reduce the
217 “central convergence” effect and highlight the long-range transport processes (Cuevas et al., 2013),
218 we adjusted the residence times using the geometric adjustment factor as proposed by Poirot and

219 Wishinski (1986).

220 The potential source regions of PBM and GOM were simulated using a Potential Source
221 Contribution Function (PSCF) approach (Zeng and Hopke, 1989). The PSCF value indicates the
222 probability that a source area contributed to the receptor site and is defined as:

$$223 \text{PSCF}_{ij} = \frac{M_{ij}}{N_{ij}} \times W_{ij} \quad (1)$$

224 M_{ij} is the total number of trajectory segment endpoints (Each trajectory segment endpoint
225 represents the estimated position of the air mass every 1 hour back in time from the receptor) in a
226 grid cell associated to PBM and GOM concentrations at the PDM Observatory higher than the
227 annual means, N_{ij} is the total number of trajectory segment endpoints in a grid cell, and W_{ij} is a
228 weighting function used to minimize the uncertainties of a small N_{ij} and described by Polissar et al
229 (2001). For the PBM and GOM PSCF analysis, 7-day back trajectories ending at the PDM
230 Observatory were calculated every 2 hours throughout the whole study period. The total trajectory
231 endpoints in the boundary layer, lower free troposphere, and middle and upper troposphere in the
232 studied domain were 152025, 285726, and 250557, respectively. The studied domain was divided
233 into 5566 grid cells of 2.0° latitude \times 2.0° longitude. Areas with high PSCF values are likely
234 enriched in atmospheric PBM and GOM and probably contribute to the elevated PBM and GOM
235 concentrations at the PDM Observatory. We caution, due to the trajectory innate spatial
236 uncertainty, meteorological parameters (e.g. precipitation, humidity), ‘trailing effect’, etc, that
237 PSCF analysis could have some uncertainties in identification of source regions (Engstrom and
238 Magnusson, 2009; Cheng et al., 2015). In this study, these factors were not evaluated and therefore
239 the identified source regions of GOM and PBM by PSCF analysis should be regarded as a
240 qualitative indication.

241

242 **3 Results and discussion**

243 **3.1 Annual, seasonal, and diel trends**

244 Averaged atmospheric GEM, PBM, and GOM concentrations at the PDM Observatory
245 during the study period were $1.86 \pm 0.27 \text{ ng m}^{-3}$, $14 \pm 10 \text{ pg m}^{-3}$, and $27 \pm 34 \text{ pg m}^{-3}$, respectively
246 (time series of GEM, PBM and GOM concentrations are in Figure S1). The level of GEM at the
247 PDM Observatory was slightly higher than the previous observations at remote sites in Europe
248 (means: $1.66 - 1.82 \text{ ng m}^{-3}$) (Slemr and Scheel, 1998; Lee et al., 1998; Kock et al., 2005) and North
249 America (means: $1.32 - 1.72 \text{ ng m}^{-3}$) (Kellerhals et al., 2003; Lan et al., 2012), but lower than that
250 observed in Asia (means: $1.60 - 3.98 \text{ ng m}^{-3}$) (Fu et al., 2015). Continuous measurements of
251 atmospheric Hg speciation at high-altitude sites are limited worldwide. The mean PBM
252 concentration at the PDM Observatory was approximately 7 times higher than at LABS (2 pg m^{-3} ,
253 23.5° N , 2862 m asl) (Sheu et al., 2010), and also higher than the summertime means at SPL (9 pg

254 m^{-3} , 40.5° N, 3230 m a.s.l) and MBO (5 pg m^{-3} , 44.0° N, 2700 m a.s.l) (Swartzendruber et al.,
255 2006;Fain et al., 2009). The annual mean GOM concentration at the PDM Observatory was
256 relatively higher than at LABS (annual mean: 12 pg m^{-3}) and SPL (summertime mean: 20 pg m^{-3})
257 (Fain et al., 2009;Sheu et al., 2010), but lower than at MBO (summertime mean: 40 pg m^{-3})
258 (Swartzendruber et al., 2006). The difference in atmospheric PBM and GOM concentrations
259 among high-altitude sites may partially reflect measurements uncertainty, but also be due to the
260 different regional and long-range Hg transport, atmospheric Hg transformations, and intrusions of
261 air from the upper troposphere and lower stratosphere.

262 Differences in GEM concentrations for different seasons were not statistically significant (t
263 test $p = 0.73$, Figure 1). The monthly mean PBM concentrations were relatively higher ($p < 0.05$)
264 in winter (December to February) and spring (March to May) than in summer (June to August)
265 and autumn (September to November), with the highest monthly mean of 21 pg m^{-3} in February
266 and the lowest monthly mean of 7 pg m^{-3} in October. This seasonal pattern is similar to the
267 observations at LABS as well as low-altitude sites in North America and China (Lan et al.,
268 2012;Fu et al., 2012;Sheu et al., 2010). Elevated winter PBM concentrations are common at
269 low-altitude sites in the Northern Hemisphere, which is likely linked to emissions from residential
270 heating, and low temperature facilitating gas-particle partitioning of atmospheric mercury, and
271 decreasing wet scavenging processes (Lan et al., 2012;Rutter and Schauer, 2007;Selin et al., 2007).
272 Monthly mean GOM concentrations were relatively higher ($p < 0.05$) in summer (mean: 38 pg m^{-3}),
273 followed by winter (mean: 25 pg m^{-3}), autumn (mean: 25 pg m^{-3}), and spring (mean: 23 pg m^{-3})
274 (Figure 1). In general, in-situ oxidation of GEM and long-range transport of GOM-enriched air
275 from the free troposphere, rather than anthropogenic emissions are the dominant sources of
276 atmospheric GOM at high-altitude sites (Sheu et al., 2010;Swartzendruber et al., 2006;Fain et al.,
277 2009).The summer maximum GOM at the PDM Observatory may indicate these processes are
278 more dominant in summer than during other seasons .

279 Atmospheric GEM, PBM, and GOM displayed well-defined diel trends at the PDM
280 Observatory (Figure 2). GEM concentrations (2-hour means) were relatively higher during
281 daytime with the maximum observed in the later afternoon (around 17:00) and minimum observed
282 in the early morning (around 5:00), and positively correlated with CO ($r^2 = 0.70$, $p < 0.01$). The
283 diel trends in PBM and GOM contrast with that of GEM, with the maximum PBM and GOM
284 concentrations (2-hour means) observed in the early morning (around 7:00) and the minimum
285 concentrations in the later afternoon (around 17:00) (Figure 2). PBM and GOM concentrations
286 were significantly anti-correlated with GEM concentrations ($r^2_{GEM-PBM} = 0.91$, $r^2_{GEM-PBM} = 0.87$,
287 $p < 0.01$ for both) and CO concentrations ($r^2_{GEM-PBM} = 0.74$, $r^2_{GEM-PBM} = 0.75$, $p < 0.01$ for both),
288 and positively correlated with each other ($r^2_{GOM-PBM} = 0.91$, $p < 0.01$) and with ozone

289 concentrations ($r^2_{\text{ozone-PBM}} = 0.93$, $r^2_{\text{ozone-GOM}} = 0.88$, $p < 0.01$ for both). The diel trends of
290 atmospheric Hg species at the PDM Observatory were similar to those at MBO and LABS (Sheu
291 et al., 2010; Swartzendruber et al., 2006), but in contrast with the GOM diel trend at SPL which
292 showed relatively higher values in the afternoon (Fain et al., 2009). The PDM Observatory is
293 frequently impacted by upslope, valley, and plain-to-mountain breezes (Gheusi et al.,
294 2011; Tsamalis et al., 2014). Elevated GEM concentrations during daytime were likely related to
295 upward transport of GEM enriched boundary layer air, whereas elevated PBM and GOM
296 concentrations at night were attributed to long-range transport of PBM and GOM-enriched air in
297 the free troposphere (see below).

298

299 3.2 High PBM events

300 We observed 44 high PBM events, which were defined as the peak concentrations higher than
301 31 pg m^{-3} , which are the 95th percentile PBM levels for the entire study. The maximum PBM
302 concentration was 98 pg m^{-3} , and was the highest value among the maximum PBM concentrations
303 ($33 - 40 \text{ pg m}^{-3}$) observed at high-altitude sites (Sheu et al., 2010; Swartzendruber et al., 2006; Fain
304 et al., 2009; Timonen et al., 2013).

305 For the 44 high PBM events, 30 events showed significant anti-correlations between PBM
306 and GEM concentrations (Supplementary Table S1). Also, the GEM levels during the 30 high
307 PBM events when peak PBM concentrations were observed were generally low with
308 concentrations less than the annual mean GEM concentrations of 1.86 ng m^{-3} . This phenomenon is
309 in contrast with PBM and GEM observations impacted by anthropogenic and biomass burning
310 emissions which showed simultaneous increases of PBM and GEM concentrations (Manolopoulos
311 et al., 2007; Song et al., 2009; Fu et al., 2011; Obrist et al., 2008). The air masses related to the 30
312 high PBM events mainly originated from the upper free troposphere over North America, Europe
313 and the Arctic (supplementary Figure S2). For the 30 high PBM events, 20 events had PBM/GOM
314 ratios higher than 1, indicating a significant proportion of depleted GEM in the upper free
315 troposphere was in the form of PBM rather than GOM. We acknowledge that PBM/GOM ratios
316 may be affected by bias in denuder GOM measurements (Gustin et al., 2013). Nevertheless our
317 observations on high PBM events appear different from previous studies at high-altitude sites
318 (note that these studies were conducted in the warm season or in the tropics) (Sheu et al.,
319 2010; Swartzendruber et al., 2006; Fain et al., 2009). A possible explanation is that most of the high
320 PBM events at the PDM Observatory were observed in the cold season which may favor the
321 production and/or accumulation of PBM in the upper free troposphere.

322 Six out of the 44 PBM events (supplementary Table S1) were probably related to direct
323 anthropogenic pollution. These events were accompanied by elevated GEM (mean = 1.96 ± 0.13

324 ng m⁻³) and CO concentrations (mean = 141 ± 26 ppb) and low GOM concentrations (mean = 22±
325 15 pg m⁻³). Also, the changes in PBM concentrations, in most cases, were positively correlated
326 with GEM and CO and anti-correlated with GOM. The back trajectory analysis suggests that the
327 air masses of these 6 PBM events were likely mixed with boundary layer air over Europe prior to
328 ending at the PDM Observatory (Supplementary Figure S3). For the remaining 8 high PBM events
329 (supplementary Table S1), no significant correlations were observed between PBM concentrations
330 and GEM. However, these events were generally accompanied by typical GEM (mean = 1.76 ±
331 0.20ng m⁻³) and CO (mean = 110 ± 11ppb) concentrations, low relative humidity (mean = 33.0 ±
332 24.1%), and elevated GOM concentrations (mean = 52 ± 29pg m⁻³). Also, a significant positive
333 correlation between PBM and GOM concentrations was observed for some of these events
334 (supplementary Table S1). Therefore, these events were not likely related to direct anthropogenic
335 pollution. The air masses related to these 8 PBM events mainly originated from the middle free
336 troposphere over the North Atlantic Ocean (Supplementary Figure S4). We therefore suggest that
337 gas-particle partitioning of GOM in the middle free troposphere over the North Atlantic Ocean and
338 during long-range transport followed by mixing with European boundary layer air prior to ending
339 at the PDM Observatory were the major cause for these 8 high PBM events.

340 Figure 3 shows two typical PBM events (PBM events #12 and #19 in supplementary Table
341 S1) with PBM and GEM anti-correlated. During the PBM event #12 (from 19 to 21 February 2012,
342 Figure 3A), the maximum PBM concentration reached up to 85 pg m⁻³, which was accompanied
343 by low GEM (1.47 ng m⁻³), low GOM (25 pg m⁻³), low atmospheric aerosol number
344 concentrations (150 nbp cm⁻³, Supplementary Table S1), and low relative humidity (6%) but
345 elevated CO concentration (128 ppb). The maximum PBM concentration during PBM event #19
346 was 40 pg m⁻³ (Figure 3B), which is lower than that of PBM event #12. PBM event #19 showed
347 elevated GOM concentrations (up to 131 pg m⁻³), higher atmospheric aerosol number
348 concentration (up to 1609 nbp cm⁻³, Supplementary Table S1) but relatively lower CO
349 concentrations (111 ppb) (Supplementary Table S1). Hysplit and Flexpart back trajectory analysis
350 shows that the air masses related to the PBM event #12 mainly originated from North America and
351 passed over high-latitude areas in the upper free troposphere prior to ending at the PDM
352 Observatory (Figure 4). PBM event #19 originated mostly from middle and upper free troposphere
353 over the Eastern North Atlantic Ocean and passed over West Europe in the middle and lower free
354 troposphere before ending at the PDM Observatory (Figure 4). We find good agreement between
355 Hysplit and Flexpart in terms of air mass geographical origin and altitude over 10 days.

356 Gas-particle partitioning of GOM and heterogeneous oxidation of GEM at aerosols surfaces
357 were suggested to be two important pathways for the formation of PBM in the atmosphere
358 (Lindberg et al., 2002;Amos et al., 2012;Subir et al., 2012). For PBM event #12, direct intrusion

359 of PBM-enriched air from the upper free troposphere likely played a dominant role. PBM event
360 #19 was likely related to gas-particle partitioning of GOM generated in the middle and upper free
361 troposphere over the North Atlantic Ocean during the transport over Western Europe. The
362 mechanisms and kinetics related to production of PBM are currently not well known. In the
363 present study, we find that PBM concentrations and PBM/GOM ratios during all the events were
364 both significantly anti-correlated with the atmospheric aerosol number concentrations ($p < 0.05$,
365 Supplementary Table S2). This result indicates that concentrations of atmospheric aerosols may
366 not play a dominant role in the formation of PBM in the middle and upper free troposphere and/or
367 during the transport to the PDM Observatory, although atmospheric aerosol number
368 concentrations observed at the PDM Observatory might be partially related to anthropogenic
369 sources in the boundary layer and not representative of that in the middle and upper free
370 troposphere. On the other hand, both PBM concentrations and PBM/GOM ratios during the high
371 PBM events were significantly anti-correlated with simulated mean temperature of air masses
372 ending at the PDM Observatory ($p < 0.05$ for both, Supplementary Table S2). Also, PBM/GOM
373 ratios were found to be significantly anti-correlated with simulated mean solar radiation flux
374 ($p < 0.05$, Supplementary Table S2). These results agree with previous studies which suggested that
375 cold temperature and lower wintertime solar radiation enhance gas-particle partitioning of GOM
376 and minimize the decomposition of PBM by photoreduction, respectively, which in turn facilitates
377 the accumulation of PBM in the middle and upper free troposphere (Lindberg et al.,
378 2002; Sprovieri et al., 2005; Rutter and Schauer, 2007; Amos et al., 2012). Previous studies also
379 suggested that aerosol uptake of atmospheric oxidants and atmospheric GEM oxidation rates may
380 be enhanced at cold temperature (Carslaw et al., 1997; Michelsen et al., 1999; Lindberg et al., 2007),
381 which in turn facilitates the production of PBM via heterogeneous GEM oxidation and
382 gas-particle partitioning of GOM.

383

384 **3.3 High GOM events**

385 High GOM events were identified as the concentrations higher the 95th percentile GOM level
386 (93 pg m^{-3}) (Supplementary Table S3). For the 61 high GOM events observed, 50 events were
387 observed with a significant anti-correlation between GOM and GEM concentrations. Also, the
388 remaining 11 high GOM events were not likely related to direct anthropogenic pollution because
389 GEM, CO, and atmospheric aerosol number concentrations were not elevated and no positive
390 correlations are observed between these parameters and GOM concentrations. We therefore
391 conclude that the high GOM events at the PDM Observatory were primarily related to in situ
392 oxidation of GEM, which is consistent with previous studies at high-altitude sites (Sheu et al.,
393 2010; Swartzendruber et al., 2006; Fain et al., 2009).

394 In general, ozone, hydroxyl radical (OH·), nitrate radical (e.g. NO, NO_y), and reactive
395 halogens (e.g. Br·, BrO, IO) are considered as potential oxidants involved in the conversion of
396 GEM to GOM in the atmosphere (Lin and Pehkonen, 1999;Goodsite et al., 2004). However, the
397 kinetics and relative contributions of these oxidants in the production of atmospheric GOM are not
398 well understood. In the present study, we observed that GOM and ozone concentrations were
399 positively correlated during 24 high GOM events (Supplementary Table S3). Meanwhile, hourly
400 mean ozone concentrations associated with GOM peaks during the 24 high GOM events ranged
401 from 41.4 to 98.5 ppb with an average value of 62.5 ppb, and were relatively higher than the
402 annual mean of 49.4 ppb. The most pronounced example was observed in 16 May, 2012 (GOM
403 Event #7, Figure 5). Clear positive correlations between GOM and ozone concentrations were also
404 reported at MBO station, USA (Swartzendruber et al., 2006;Timonen et al., 2013), but elevated
405 ozone concentrations as high as 105 ppb (5-min mean) during high GOM events #7 were not
406 observed in any previous observations at high-altitude sites. The highly elevated ozone
407 concentrations as well as low CO concentrations and relative humidity demonstrate that event #7
408 was mainly related to intrusions from the upper free troposphere. This assessment was further
409 supported by the backward trajectory analysis which shows the major origins of air masses from
410 the upper free troposphere over the Arctic region and North America (Figure 6). At the night
411 during event #7 when an upper tropospheric intrusion dominated, ozone concentrations were
412 significantly anti-correlated with GEM ($GEM = -9.3 \text{ pg m}^{-3}/\text{ppb} \times O_3 \text{ ppb} + 2190 \text{ pg m}^{-3}$, $r^2 = 0.72$
413 $p < 0.01$) and positively correlated with GOM concentrations ($GOM = 2.69 \text{ pg m}^{-3}/\text{ppb} \times O_3 \text{ ppb} -$
414 113 pg m^{-3} , $r^2 = 0.96$, $p < 0.01$). The correlations indicated a total depletion of GEM in the upper
415 free troposphere when ozone exceeds 235 ppb, and corresponding GOM concentrations up to
416 approximately 520 pg m⁻³. This finding is in agreement with aircraft observations of GEM and
417 GOM+PBM fractions in the upper free troposphere and tropopause (Talbot et al., 2007;Lyman and
418 Jaffe, 2012).

419 For the 24 high GOM events positively correlated with ozone, many air masses (10 out of the
420 24 high GOM events) originated from the upper troposphere over the Arctic region and the
421 remainder from the middle troposphere over the North Atlantic Ocean (Supplementary Figure S5).
422 This implies that the frequent southward intrusion of upper tropospheric air from the Arctic region
423 may be an important source of high GOM levels at the PDM Observatory and mid-latitudes. In
424 general, atmospheric ozone levels exhibit a clear vertical profile with concentrations increasing
425 with altitude (Browell et al., 2003;Chevalier et al., 2007), and this may explain well the observed
426 positive correlation between GOM and ozone concentrations. However, this by no means
427 demonstrates that ozone is the exclusive oxidant during these events. In fact, nitrate radical (e.g.
428 NO, NO_y) levels were found to be tightly correlated with ozone in the upper free troposphere (Gao

429 et al., 2014;Kohler et al., 2013;Slemr et al., 2009). The vertical profiles of hydroxyl radical and
430 reactive halogens are not well established (Brune et al., 1998). However, elevated BrO and
431 OH· levels were reported in the middle and upper free troposphere by previous studies (Brune et
432 al., 1998;Fitzenberger et al., 2000). Therefore, these oxidants could also contribute to the
433 oxidation of GEM in the middle and upper free troposphere.

434 Nine of the high GOM events showed anti-correlations between GOM and ozone
435 concentrations (Supplementary Table S3), which are in contrast with GOM events influenced by
436 the middle and upper tropospheric air. Back trajectory analysis suggests that these events were
437 influenced by air masses originated from and/or passed over the North Atlantic in the lower free
438 troposphere (Supplementary Figure S6). This type of events was similar as that observed in the
439 Pacific Ocean MBL (Timonen et al., 2013;Laurier et al., 2003), indicating a decrease in ozone
440 concentration is a general feature of GOM production in lower free troposphere over oceans and
441 MBL. It is possible that reactive halogen and hydroxyl radicals were involved in this type of GOM
442 events, the formation of which in the MBL over oceans were thought to deplete atmospheric
443 ozone (Bloss et al., 2003;Obrist et al., 2011;Read et al., 2008).

444 High GOM events were also reported to be related to oxidation of GEM in MBL over the
445 Arctic region during Polar spring and Pacific Ocean during warm seasons (Steffen et al.,
446 2008;Timonen et al., 2013). For the high GOM events in the present study, we did not observe
447 clear evidence for the sources of GOM from the MBL over the Arctic region or the North Atlantic
448 Ocean. Therefore, the oxidation of GEM in the free troposphere was likely the predominant source
449 of high GOM at the PDM Observatory. The remaining 28 high GOM events (Supplementary Table
450 S3), with GOM poorly correlated with ozone and GEM concentrations, probably reflect the
451 combined effect of intrusions of GOM-enriched air from middle and upper free troposphere, lower
452 free troposphere over the Atlantic Ocean and mixing of boundary layer air over Europe during
453 long-range transport.

454

455 **3.4 Seasonal trends of high PBM and GOM events**

456 The high PBM events were predominantly observed in winter and spring (from November to
457 April, Figure 7), which accounted for approximately 80% of the total high PBM events. In
458 contrast, high GOM events were predominantly (~69%) observed in the summer and autumn
459 (from May to October). The monthly variations in the frequencies of high PBM and GOM events
460 were consistent with the monthly means of PBM and GOM concentrations, respectively. This is
461 the first observation suggesting that high PBM and GOM events in the free troposphere in the
462 middle latitude display distinct seasonal patterns (t test: $p < 0.05$).

463 ARTs related to the high PBM events in spring and winter showed maximum values in the

464 upper free troposphere over North America (accounting for 35% of total high PBM ARTs),
465 followed by the middle free troposphere over the North Atlantic Ocean (29%), the upper free
466 troposphere over the Arctic region (22%) and the middle free troposphere over the Europe (13%)
467 (Figure 8). The maximum high PBM ARTs over North America in spring and winter were partly
468 attributed to increasing origins of air masses from this region under the influence of westerlies in
469 the mid-latitude (Figure 9). Additionally, the ratios of high PBM ARTs to total ARTs over North
470 America were also elevated in winter and spring compared to summer and spring. It is noteworthy
471 that the ratios of high PBM ARTs to total ARTs in winter and spring were significantly higher (t
472 test, $p < 0.05$) than that in summer and autumn over all the studied regions (Figure 9). This result
473 may imply that the middle and upper free troposphere of the Northern Hemisphere may be more
474 enriched in PBM in spring and winter than in summer and autumn. This conclusion is consistent
475 with the modeling result at low-altitude sites in North America which was likely due to cold
476 season subsidence of PBM enriched air from the upper troposphere and lower stratosphere (Amos
477 et al., 2012). There are currently no observations regarding the seasonal trends of atmospheric
478 PBM in the middle and upper free troposphere of the Northern Hemisphere. In spring and winter
479 increasing PBM concentrations the middle and upper free troposphere of the Northern Hemisphere
480 are apparently in contrast with the lower atmospheric aerosol concentrations observed at the PDM
481 Observatory as well as other high altitudes in Europe and North America (Browell et al.,
482 2003; Asmi et al., 2011). We therefore proposed that factors other than atmospheric aerosols
483 played a more important role in the seasonal variations of high PBM events at **the PDM**
484 **Observatory**. As we discussed earlier, cold temperature and lower solar radiation may favor the
485 production and accumulation of PBM in the free troposphere. Northern Hemisphere high-latitudes
486 are characterized by relatively lower air temperature and solar radiation during the cold season,
487 which may facilitate the production and accumulation of PBM in the middle and upper
488 troposphere in cold season and explain our seasonal variations in atmospheric PBM concentrations.
489 In summer the highest high PBM ARTs were observed in the lower and middle free troposphere
490 over the North Atlantic Ocean (accounting for 72% of total ARTs in summer). The lower and
491 middle free troposphere over the North Atlantic Ocean in summer produced many high GOM
492 events (more details below), which are responsible for the highest ARTs associated with high
493 PBM events in this region via gas-particle partitioning of atmospheric GOM.

494 ARTs related to the high GOM events showed maximum values over the North Atlantic
495 Ocean regardless of seasons (accounting for 62-84% of total residence times). High GOM ARTs
496 over the North Atlantic Ocean mainly correspond to the lower and middle free troposphere (Figure
497 10). In summer when most of high GOM events were observed, high GOM ARTs showed
498 maximum values in the lower free troposphere over the subtropical North Atlantic Ocean.

499 Maximum high GOM ARTs were mainly observed in the middle free troposphere over the
500 temperate and sub-arctic North Atlantic Ocean in spring and autumn (Figure 10 and 11). The
501 maximum high GOM ARTs over the subtropical North Atlantic Ocean in summer were partially
502 attributed to frequent origins of air masses from this region (Figure 11). Also, it is found that the
503 ratios of high GOM ARTs to total ARTs over the subtropical North Atlantic Ocean in summer
504 were up to an order of magnitude higher than that in other seasons over the temperate and
505 sub-arctic North Atlantic Ocean in summer. These results imply that the lower free troposphere
506 over the subtropical North Atlantic Ocean may be of specific significance for the production of
507 GOM in summer. For other seasons, the maximum high GOM ARTs over the temperate and
508 sub-arctic North Atlantic Ocean were related to frequent intrusions of air masses from the middle
509 and upper free troposphere (Figure 10 and 11).

510 The summer maximum high GOM events are also similar to observations at the Dead Sea,
511 Israel (Moore et al., 2013), which were associated with elevated BrO concentrations in the MBL.
512 Many recent studies also suggested that other oxidants such as hydroxyl radical ($\text{OH}\cdot$), iodine
513 oxides (IO), chlorine atoms ($\text{Cl}\cdot$), ozone, nitrogen oxides (e.g. NO_2) should be also involved in the
514 production of GOM in the atmosphere (Dibble et al., 2012; Wang et al., 2014; Weiss-Penzias et al.,
515 2015). Previous studies observed that $\text{OH}\cdot$, IO and NO_2 concentrations in the MBL and lower free
516 troposphere over the subtropical and tropical North Atlantic Ocean are highest in summer
517 (Spivakovsky et al., 2000; Savage et al., 2004; Wang et al., 2014; Martin et al., 2008), which may
518 explain the maximum summer high GOM ARTs in the lower free troposphere over the subtropical
519 North Atlantic Ocean. On the other hand, atmospheric oxidants in the middle and upper free
520 troposphere also display clear seasonal cycles. For instance, Fitzenberger et al.(2000) observed
521 that BrO concentrations in the middle and upper free troposphere over the Arctic region were
522 relatively higher in summer than in winter. Additionally, previous studies also suggested that
523 tropospheric column ozone and $\text{OH}\cdot$ concentrations in the Northern Hemisphere are highest in
524 summer (Spivakovsky et al., 2000; Liu et al., 2006). These oxidants may favor the in situ
525 production of GOM in the middle and upper free troposphere in summer.

526

527 **3.5 Potential source regions of PBM and GOM in different layers of troposphere**

528 The major potential source regions of PBM at the PDM Observatory were located over the
529 temperate and sub-arctic North Atlantic Ocean and over Northwest Europe, whereas the major
530 potential source regions of GOM at the PDM Observatory were located in the subtropical North
531 Atlantic Ocean (Figure 12). The PSCF analysis regarding the different atmospheric layers suggests
532 that major source regions of PBM and GOM were both from the middle and upper free
533 troposphere over the temperate and sub-arctic North Atlantic Ocean, Arctic region, North America,

534 and Northwest Europe, which were followed by the lower free troposphere over the subtropical
535 North Atlantic Ocean. On the other hand, the boundary layer over the Atlantic Ocean, Europe, and
536 North America played a minimal role in the sources of PBM and GOM at the PDM Observatory. It
537 should be pointed out that, owing to the trailing effect (areas upwind and downwind of actual
538 source regions are likely identified as possible source regions), some of the identified source
539 regions of PBM and GOM might be overestimated. As we discussed earlier, many high PBM and
540 GOM events were related to air masses that originated from or traveled in the upper free
541 troposphere over the Arctic region and sub-arctic North America. The transport of these air masses
542 frequently took a southward route (Stohl et al., 2000), which may overestimate the contributions
543 of source regions over the temperate and sub-arctic North Atlantic Ocean and Northwest Europe.

544

545 **4 Conclusions**

546 In the present study, we consider one full year of atmospheric Hg speciation observations at
547 the high-altitude Pic du Midi (PDM) Observatory, located in the middle latitudes. Unlike previous
548 studies at other high-altitude sites (mainly conducted in warm seasons or in the tropics), we
549 observed multiple high PBM events (up to 98 pg m⁻³) in addition to multiple high GOM events
550 (up to 295 pg m⁻³), which were mainly related to in situ atmospheric transformations. The seasonal
551 variations in the occurrence of high PBM and GOM events were significantly different with most
552 of the high PBM and GOM events occurring in cold seasons (winter and spring) and warm
553 seasons (summer and autumn), respectively. Our study suggests that an important fraction of
554 depleted GEM is in the form of PBM in the middle and upper troposphere in cold seasons. These
555 findings should be taken into account by modeling approaches to better understand the fate of Hg
556 in the global atmosphere. Furthermore, our results suggest that the sources of high PBM and GOM
557 events were also different. High PBM events in cold seasons were mainly related to intrusions
558 from the upper troposphere over temperate and sub-arctic North American and Arctic regions as
559 well as the middle troposphere over the temperate North Atlantic Ocean and Europe. On the other
560 hand, high GOM events were attributed to in situ production in the middle and lower free
561 troposphere over the subtropical North Atlantic Ocean. These seasonal and regional patterns may
562 be caused by a combination of factors including variations of atmospheric oxidants and
563 meteorological parameters (e.g. temperature and solar radiation). As GOM and PBM are readily
564 deposited to Earth's surfaces, the frequent export of PBM- and GOM-enriched air from North
565 America, the Arctic region and the North Atlantic Ocean are expected to enhance wet and dry
566 deposition and cause environmental risk of mercury in European ecosystems. This should be
567 further evaluated using modeling approaches.

568

569 **Supplementary material:**

570 Tables of the identified 44 high PBM events, 61 high GOM events and Pearson's correlation
571 analysis between PBM and meteorological parameters and atmospheric pollutants are shown in
572 Tables S1-S3.

573 Time series of atmospheric Hg speciation, backward trajectories of the 30 high PBM events
574 related to upper tropospheric intrusions, backward trajectories of the 6 anthropogenic impacted
575 high PBM events, backward trajectories of the 8 mixed high PBM events, backward trajectories of
576 the 24 high GOM events related to intrusions from middle and upper troposphere, backward
577 trajectories of the 9 high GOM events related to marine free tropospheric air are shown in Figure
578 S1-S6.

579

580

581 **Acknowledgments:** This work was supported by research grant ERC-2010-StG_20091028 from
582 the European Research Council and the National Science Foundation of China (41473025,
583 41273145). We acknowledge technical support from the UMS 831 Pic du Midi observatory team.
584 Beyond mercury speciation, other observational data were provided by the PAES atmospheric
585 monitoring service supported by CNRS-INSU.

586

587 **References**

588 Amos, H. M., Jacob, D. J., Holmes, C. D., Fisher, J. A., Wang, Q., Yantosca, R. M., Corbitt, E. S.,
589 Galarneau, E., Rutter, A. P., Gustin, M. S., Steffen, A., Schauer, J. J., Graydon, J. A., St Louis, V. L.,
590 Talbot, R. W., Edgerton, E. S., Zhang, Y., and Sunderland, E. M.: Gas-particle partitioning of
591 atmospheric Hg(II) and its effect on global mercury deposition, *Atmos Chem Phys*, 12, 591-603, DOI
592 10.5194/acp-12-591-2012, 2012.

593 Asmi, A., Wiedensohler, A., Laj, P., Fjaeraa, A. M., Sellegri, K., Birmili, W., Weingartner, E.,
594 Baltensperger, U., Zdimal, V., Zikova, N., Putaud, J. P., Marinoni, A., Tunved, P., Hansson, H. C.,
595 Fiebig, M., Kivekas, N., Lihavainen, H., Asmi, E., Ulevicius, V., Aalto, P. P., Swietlicki, E., Kristensson,
596 A., Mihalopoulos, N., Kalivitis, N., Kalapov, I., Kiss, G., de Leeuw, G., Henzing, B., Harrison, R. M.,
597 Beddows, D., O'Dowd, C., Jennings, S. G., Flentje, H., Weinhold, K., Meinhardt, F., Ries, L., and
598 Kulmala, M.: Number size distributions and seasonality of submicron particles in Europe 2008-2009,
599 *Atmos Chem Phys*, 11, 5505-5538, DOI 10.5194/acp-11-5505-2011, 2011.

600 Bloss, W. J., Gravestock, T. J., Heard, D. E., Ingham, T., Johnson, G. P., and Lee, J. D.: Application of a
601 compact all solid-state laser system to the in situ detection of atmospheric OH, HO₂, NO and IO by
602 laser-induced fluorescence, *J Environ Monitor*, 5, 21-28, Doi 10.1039/B208714f, 2003.

603 Browell, E. V., Hair, J. W., Butler, C. F., Grant, W. B., DeYoung, R. J., Fenn, M. A., Brackett, V. G.,
604 Clayton, M. B., Brasseur, L. A., Harper, D. B., Ridley, B. A., Klonecki, A. A., Hess, P. G., Emmons, L.
605 K., Tie, X. X., Atlas, E. L., Cantrell, C. A., Wimmers, A. J., Blake, D. R., Coffey, M. T., Hannigan, J.
606 W., Dibb, J. E., Talbot, R. W., Flocke, F., Weinheimer, A. J., Fried, A., Wert, B., Snow, J. A., and Lefer,
607 B. L.: Ozone, aerosol, potential vorticity, and trace gas trends observed at high-latitudes over North
608 America from February to May 2000, *J Geophys Res-Atmos*, 108, Artn 8369
609 Doi 10.1029/2001jd001390, 2003.

610 Brune, W. H., Faloon, I. C., Tan, D., Weinheimer, A. J., Campos, T., Ridley, B. A., Vay, S. A., Collins,
611 J. E., Sachse, G. W., Jaegle, L., and Jacob, D. J.: Airborne in-situ OH and HO₂ observations in the
612 cloud-free troposphere and lower stratosphere during SUCCESS, *Geophys Res Lett*, 25, 1701-1704,

613 Doi 10.1029/97gl03098, 1998.

614 Carslaw, K. S., Peter, T., and Clegg, S. L.: Modeling the composition of liquid stratospheric aerosols,
615 *Rev Geophys*, 35, 125-154, Doi 10.1029/97rg00078, 1997.

616 Cheng, I., Xu, X., and Zhang, L.: Overview of receptor-based source apportionment studies for
617 speciated atmospheric mercury, *Atmos Chem Phys*, 15, 7877-7895, 2015.

618 Chevalier, A., Gheusi, F., Delmas, R., Ordonez, C., Sarrat, C., Zbinden, R., Thouret, V., Athier, G., and
619 Cousin, J. M.: Influence of altitude on ozone levels and variability in the lower troposphere: a
620 ground-based study for western Europe over the period 2001-2004, *Atmos Chem Phys*, 7, 4311-4326,
621 2007.

622 Cuevas, E., Gonzalez, Y., Rodriguez, S., Guerra, J. C., Gomez-Pelaez, A. J., Alonso-Perez, S., Bustos,
623 J., and Milford, C.: Assessment of atmospheric processes driving ozone variations in the subtropical
624 North Atlantic free troposphere, *Atmos Chem Phys*, 13, 1973-1998, 10.5194/acp-13-1973-2013, 2013.

625 Dibble, T. S., Zelic, M. J., and Mao, H.: Thermodynamics of reactions of ClHg and BrHg radicals with
626 atmospherically abundant free radicals, *Atmos Chem Phys*, 12, 10271-10279,
627 10.5194/acp-12-10271-2012, 2012.

628 HYSPLIT (HYbrid Single-Particle Lagrangian Integrated Trajectory) Model access via NOAA ARL
629 READY Website (<http://www.arl.noaa.gov/HYSPLIT.php>). NOAA Air Resources Laboratory, College
630 Park, MD.

631 Driscoll, C. T., Mason, R. P., Chan, H. M., Jacob, D. J., and Pirrone, N.: Mercury as a Global Pollutant:
632 Sources, Pathways, and Effects, *Environmental Science & Technology*, 47, 4967-4983, Doi
633 10.1021/Es305071v, 2013.

634 Engstrom, A., and Magnusson, L.: Estimating trajectory uncertainties due to flow dependent errors in
635 the atmospheric analysis, *Atmos Chem Phys*, 9, 8857-8867, 2009.

636 Fain, X., Obrist, D., Hallar, A. G., Mccubbin, I., and Rahn, T.: High levels of reactive gaseous mercury
637 observed at a high elevation research laboratory in the Rocky Mountains, *Atmos Chem Phys*, 9,
638 8049-8060, 2009.

639 Fitzenberger, R., Bosch, H., Camy-Peyret, C., Chipperfield, M. P., Harder, H., Platt, U., Sinnhuber, B.
640 M., Wagner, T., and Pfeilsticker, K.: First profile measurements of tropospheric BrO, *Geophys Res Lett*,
641 27, 2921-2924, Doi 10.1029/2000gl011531, 2000.

642 Fu, X., Feng, X., Sommar, J., and Wang, S.: A review of studies on atmospheric mercury in China, *Sci
643 Total Environ*, 421-422, 73-81, 10.1016/j.scitotenv.2011.09.089, 2012.

644 Fu, X. W., Feng, X. B., Qiu, G. L., Shang, L. H., and Zhang, H.: Speciated atmospheric mercury and its
645 potential source in Guiyang, China, *Atmos Environ*, 45, 4205-4212, DOI
646 10.1016/j.atmosenv.2011.05.012, 2011.

647 Fu, X. W., Zhang, H., Yu, B., Wang, X., Lin, C. J., and Feng, X. B.: Observations of atmospheric
648 mercury in China: a critical review, *Atmos. Chem. Phys.*, 15, 9455-9476, 10.5194/acp-15-9455-2015,
649 2015.

650 Gao, R. S., Rosenlof, K. H., Fahey, D. W., Wennberg, P. O., Hints, E. J., and Hanisco, T. F.: OH in the
651 tropical upper troposphere and its relationships to solar radiation and reactive nitrogen, *Journal of
652 Atmospheric Chemistry*, 71, 55-64, DOI 10.1007/s10874-014-9280-2, 2014.

653 Gheusi, F., Ravetta, F., Delbarre, H., Tsamalis, C., Chevalier-Rosso, A., Leroy, C., Augustin, P., Delmas,
654 R., Ancellet, G., Athier, G., Bouchou, P., Campistron, B., Cousin, J. M., Fourmentin, M., and
655 Meyerfeld, Y.: Pic 2005, a field campaign to investigate low-tropospheric ozone variability in the
656 Pyrenees, *Atmos Res*, 101, 640-665, DOI 10.1016/j.atmosres.2011.04.014, 2011.

657 Goodsite, M. E., Plane, J. M. C., and Skov, H.: A theoretical study of the oxidation of Hg-0 to HgBr₂ in
658 the troposphere, *Environmental Science & Technology*, 38, 1772-1776, Doi 10.1021/Es034680s, 2004.

659 Gustin, M. S., Weiss-Penzias, P. S., and Peterson, C.: Investigating sources of gaseous oxidized
660 mercury in dry deposition at three sites across Florida, USA, *Atmos Chem Phys*, 12, 9201-9219,
661 10.5194/acp-12-9201-2012, 2012.

662 Gustin, M. S., Huang, J. Y., Miller, M. B., Peterson, C., Jaffe, D. A., Ambrose, J., Finley, B. D., Lyman,
663 S. N., Call, K., Talbot, R., Feddersen, D., Mao, H. T., and Lindberg, S. E.: Do We Understand What the
664 Mercury Speciation Instruments Are Actually Measuring? Results of RAMIX, *Environmental Science
665 & Technology*, 47, 7295-7306, Doi 10.1021/Es3039104, 2013.

666 Henne, S., Brunner, D., Folini, D., Solberg, S., Klausen, J., and Buchmann, B.: Assessment of
667 parameters describing representativeness of air quality in-situ measurement sites, *Atmos Chem Phys*,
668 10, 3561-3581, 2010.

669 Holmes, C. D., Jacob, D. J., Corbitt, E. S., Mao, J., Yang, X., Talbot, R., and Slemr, F.: Global
670 atmospheric model for mercury including oxidation by bromine atoms, *Atmos Chem Phys*, 10,
671 12037-12057, DOI 10.5194/acp-10-12037-2010, 2010.

672 Huang, J. Y., Miller, M. B., Weiss-Penzias, P., and Gustin, M. S.: Comparison of Gaseous Oxidized Hg
673 Measured by KCl-Coated Denuders, and Nylon and Cation Exchange Membranes, *Environmental
674 Science & Technology*, 47, 7307-7316, Doi 10.1021/Es4012349, 2013.

675 Kellerhals, M., Beauchamp, S., Belzer, W., Blanchard, P., Froude, F., Harvey, B., McDonald, K., Pilote,
676 M., Poissant, L., Puckett, K., Schroeder, B., Steffen, A., and Tordon, R.: Temporal and spatial
677 variability of total gaseous mercury in Canada: results from the Canadian Atmospheric Mercury
678 Measurement Network (CAMNet), *Atmos Environ*, 37, 1003-1011, Pii S1352-2310(02)00917-2
679 Doi 10.1016/S1352-2310(02)00917-2, 2003.

680 Kock, H. H., Bieber, E., Ebinghaus, R., Spain, T. G., and Thees, B.: Comparison of long-term trends
681 and seasonal variations of atmospheric mercury concentrations at the two European coastal monitoring
682 stations Mace Head, Ireland, and Zingst, Germany, *Atmos Environ*, 39, 7549-7556, DOI
683 10.1016/j.atmosenv.2005.02.059, 2005.

684 Kohler, M. O., Radel, G., Shine, K. P., Rogers, H. L., and Pyle, J. A.: Latitudinal variation of the effect
685 of aviation NO_x emissions on atmospheric ozone and methane and related climate metrics, *Atmos
686 Environ*, 64, 1-9, DOI 10.1016/j.atmosenv.2012.09.013, 2013.

687 Lan, X., Talbot, R., Castro, M., Perry, K., and Luke, W.: Seasonal and diurnal variations of atmospheric
688 mercury across the US determined from AMNet monitoring data, *Atmos Chem Phys*, 12, 10569-10582,
689 DOI 10.5194/acp-12-10569-2012, 2012.

690 Landis, M. S., Stevens, R. K., Schaedlich, F., and Prestbo, E. M.: Development and characterization of
691 an annular denuder methodology for the measurement of divalent inorganic reactive gaseous mercury
692 in ambient air, *Environmental Science & Technology*, 36, 3000-3009, Doi 10.1021/Es015887t, 2002.

693 Laurier, F. J. G., Mason, R. P., Whalin, L., and Kato, S.: Reactive gaseous mercury formation in the
694 North Pacific Ocean's marine boundary layer: A potential role of halogen chemistry, *J Geophys
695 Res-Atmos*, 108, Artn 4529
696 Doi 10.1029/2003jd003625, 2003.

697 Lee, D. S., Dollard, G. J., and Pepler, S.: Gas-phase mercury in the atmosphere of the United Kingdom,
698 *Atmos Environ*, 32, 855-864, Doi 10.1016/S1352-2310(97)00316-6, 1998.

699 Lee, D. S., Nemitz, E., Fowler, D., and Kingdon, R. D.: Modelling atmospheric mercury transport and
700 deposition across Europe and the UK, *Atmos Environ*, 35, 5455-5466, Doi

701 10.1016/S1352-2310(01)00284-9, 2001.

702 Lin, C. J., and Pehkonen, S. O.: The chemistry of atmospheric mercury: a review, *Atmos Environ*, 33,
703 2067-2079, Doi 10.1016/S1352-2310(98)00387-2, 1999.

704 Lin, C. J., Pan, L., Streets, D. G., Shetty, S. K., Jang, C., Feng, X., Chu, H. W., and Ho, T. C.:
705 Estimating mercury emission outflow from East Asia using CMAQ-Hg, *Atmos Chem Phys*, 10,
706 1853-1864, 2010.

707 Lindberg, S., Bullock, R., Ebinghaus, R., Engstrom, D., Feng, X. B., Fitzgerald, W., Pirrone, N.,
708 Prestbo, E., and Seigneur, C.: A synthesis of progress and uncertainties in attributing the sources of
709 mercury in deposition, *Ambio*, 36, 19-32, 2007.

710 Lindberg, S. E., Brooks, S., Lin, C. J., Scott, K. J., Landis, M. S., Stevens, R. K., Goodsite, M., and
711 Richter, A.: Dynamic oxidation of gaseous mercury in the Arctic troposphere at polar sunrise,
712 *Environmental Science & Technology*, 36, 1245-1256, Doi 10.1021/Es0111941, 2002.

713 Liu, X., Chance, K., Sioris, C. E., Kurosu, T. P., Spurr, R. J. D., Martin, R. V., Fu, T. M., Logan, J. A.,
714 Jacob, D. J., Palmer, P. I., Newchurch, M. J., Megretskaia, I. A., and Chatfield, R. B.: First directly
715 retrieved global distribution of tropospheric column ozone from GOME: Comparison with the
716 GEOS-CHEM model, *J Geophys Res-Atmos*, 111, Artn D02308
717 Doi 10.1029/2005jd006564, 2006.

718 Lyman, S. N., Jaffe, D. A., and Gustin, M. S.: Release of mercury halides from KCl denuders in the
719 presence of ozone, *Atmos Chem Phys*, 10, 8197-8204, DOI 10.5194/acp-10-8197-2010, 2010.

720 Lyman, S. N., and Jaffe, D. A.: Formation and fate of oxidized mercury in the upper troposphere and
721 lower stratosphere, *Nat Geosci*, 5, 114-117, Doi 10.1038/Ngeo1353, 2012.

722 Malcolm, E. G., and Keeler, G. J.: Evidence for a sampling artifact for particulate-phase mercury in the
723 marine atmosphere, *Atmos Environ*, 41, 3352-3359, DOI 10.1016/j.atmosenv.2006.12.024, 2007.

724 Manolopoulos, H., Snyder, D. C., Schauer, J. J., Hill, J. S., Turner, J. R., Olson, M. L., and Krabbenhoft,
725 D. P.: Sources of speciated atmospheric mercury at a residential neighborhood impacted by industrial
726 sources, *Environmental Science & Technology*, 41, 5626-5633, Doi 10.1021/Es0700348, 2007.

727 Martin, M. V., Honrath, R. E., Owen, R. C., and Li, Q. B.: Seasonal variation of nitrogen oxides in the
728 central North Atlantic lower free troposphere, *J Geophys Res-Atmos*, 113, Artn D17307
729 10.1029/2007jd009688, 2008.

730 McClure, C. D., Jaffe, D. A., and Edgerton, E. S.: Evaluation of the KCl Denuder Method for Gaseous
731 Oxidized Mercury using HgBr₂ at an In-Service AMNet Site, *Environmental Science & Technology*,
732 48, 11437-11444, Doi 10.1021/Es502545k, 2014.

733 Michelsen, H. A., Spivakovsky, C. M., and Wofsy, S. C.: Aerosol-mediated partitioning of stratospheric
734 Cl_y and NO_y at temperatures above 200 K, *Geophys Res Lett*, 26, 299-302, Doi
735 10.1029/1998gl900281, 1999.

736 Moore, C. W., Obrist, D., and Luria, M.: Atmospheric mercury depletion events at the Dead Sea:
737 Spatial and temporal aspects, *Atmos Environ*, 69, 231-239, DOI 10.1016/j.atmosenv.2012.12.020,
738 2013.

739 Murphy, D. M., Thomson, D. S., and Mahoney, T. M. J.: In situ measurements of organics, meteoritic
740 material, mercury, and other elements in aerosols at 5 to 19 kilometers, *Science*, 282, 1664-1669, DOI
741 10.1126/science.282.5394.1664, 1998.

742 Murphy, D. M., Hudson, P. K., Thomson, D. S., Sheridan, P. J., and Wilson, J. C.: Observations of
743 mercury-containing aerosols, *Environmental Science & Technology*, 40, 3163-3167, Doi
744 10.1021/Es052385x, 2006.

745 Obrist, D., Moosmuller, H., Schurmann, R., Chen, L. W. A., and Kreidenweis, S. M.: Particulate-phase
746 and gaseous elemental mercury emissions during biomass combustion: Controlling factors and
747 correlation with particulate matter emissions, *Environmental Science & Technology*, 42, 721-727, Doi
748 10.1021/Es071279n, 2008.

749 Obrist, D., Tas, E., Peleg, M., Matveev, V., Fain, X., Asaf, D., and Luria, M.: Bromine-induced
750 oxidation of mercury in the mid-latitude atmosphere, *Nat Geosci*, 4, 22-26, Doi 10.1038/Ngeo1018,
751 2011.

752 Pirrone, N., Cinnirella, S., Feng, X., Finkelman, R. B., Friedli, H. R., Leaner, J., Mason, R., Mukherjee,
753 A. B., Stracher, G. B., Streets, D. G., and Telmer, K.: Global mercury emissions to the atmosphere from
754 anthropogenic and natural sources, *Atmos Chem Phys*, 10, 5951-5964, DOI 10.5194/acp-10-5951-2010,
755 2010.

756 Poirot, R. L., and Wishinski, P. R.: Visibility, Sulfate and Air-Mass History Associated with the
757 Summertime Aerosol in Northern Vermont, *Atmos Environ*, 20, 1457-1469, Doi
758 10.1016/0004-6981(86)90018-1, 1986.

759 Polissar, A. V., Hopke, P. K., and Harris, J. M.: Source regions for atmospheric aerosol measured at
760 Barrow, Alaska, *Environmental Science & Technology*, 35, 4214-4226, Doi 10.1021/Es0107529, 2001.

761 Read, K. A., Mahajan, A. S., Carpenter, L. J., Evans, M. J., Faria, B. V. E., Heard, D. E., Hopkins, J. R.,
762 Lee, J. D., Moller, S. J., Lewis, A. C., Mendes, L., McQuaid, J. B., Oetjen, H., Saiz-Lopez, A., Pilling,
763 M. J., and Plane, J. M. C.: Extensive halogen-mediated ozone destruction over the tropical Atlantic
764 Ocean, *Nature*, 453, 1232-1235, Doi 10.1038/Nature07035, 2008.

765 Rutter, A. P., and Schauer, J. J.: The effect of temperature on the gas-particle partitioning of reactive
766 mercury in atmospheric aerosols, *Atmos Environ*, 41, 8647-8657, DOI
767 10.1016/j.atmosenv.2007.07.024, 2007.

768 Savage, N. H., Law, K. S., Pyle, J. A., Richter, A., Nuss, H., and Burrows, J. P.: Using GOME NO2
769 satellite data to examine regional differences in TOMCAT model performance, *Atmos Chem Phys*, 4,
770 1895-1912, 2004.

771 Schroeder, W. H., and Munthe, J.: Atmospheric mercury - An overview, *Atmos Environ*, 32, 809-822,
772 Doi 10.1016/S1352-2310(97)00293-8, 1998.

773 Selin, N. E., Jacob, D. J., Park, R. J., Yantosca, R. M., Strode, S., Jaegle, L., and Jaffe, D.: Chemical
774 cycling and deposition of atmospheric mercury: Global constraints from observations, *J Geophys*
775 *Res-Atmos*, 112, Artn D02308
776 Doi 10.1029/2006jd007450, 2007.

777 Selin, N. E., Jacob, D. J., Yantosca, R. M., Strode, S., Jaegle, L., and Sunderland, E. M.: Global 3-D
778 land-ocean-atmosphere model for mercury: Present-day versus preindustrial cycles and anthropogenic
779 enrichment factors for deposition, *Global Biogeochem Cy*, 22, Artn Gb2011
780 10.1029/2007gb003040, 2008.

781 Sheu, G. R., Lin, N. H., Wang, J. L., Lee, C. T., Yang, C. F. O., and Wang, S. H.: Temporal distribution
782 and potential sources of atmospheric mercury measured at a high-elevation background station in
783 Taiwan, *Atmos Environ*, 44, 2393-2400, DOI 10.1016/j.atmosenv.2010.04.009, 2010.

784 Slemr, F., and Scheel, H. E.: Trends in atmospheric mercury concentrations at the summit of the Wank
785 mountain, southern Germany, *Atmos Environ*, 32, 845-853, Doi 10.1016/S1352-2310(97)00131-3,
786 1998.

787 Slemr, F., Ebinghaus, R., Brenninkmeijer, C. A. M., Hermann, M., Kock, H. H., Martinsson, B. G.,
788 Schuck, T., Sprung, D., van Velthoven, P., Zahn, A., and Ziereis, H.: Gaseous mercury distribution in

789 the upper troposphere and lower stratosphere observed onboard the CARIBIC passenger aircraft,
790 *Atmos Chem Phys*, 9, 1957-1969, 2009.

791 Slemr, F., Weigelt, A., Ebinghaus, R., Brenninkmeijer, C., Baker, A., Schuck, T., Rauthe-Schoch, A.,
792 Riede, H., Leedham, E., Hermann, M., van Velthoven, P., Oram, D., O'Sullivan, D., Dyroff, C., Zahn,
793 A., and Ziereis, H.: Mercury Plumes in the Global Upper Troposphere Observed during Flights with the
794 CARIBIC Observatory from May 2005 until June 2013, *Atmosphere-Basel*, 5, 342-369, Doi
795 10.3390/Atmos5020342, 2014.

796 Slemr, F., Weigelt, A., Ebinghaus, R., Kock, H. H., Bödewadt, J., Brenninkmeijer, C. A. M.,
797 Rauthe-Schöch, A., Weber, S., Hermann, M., Zahn, A., and Martinsson, B.: Atmospheric mercury
798 measurements onboard the CARIBIC passenger aircraft, *Atmos. Meas. Tech. Discuss.*, 2016, 1-25,
799 10.5194/amt-2015-376, 2016.

800 Song, X. J., Cheng, I., and Lu, J.: Annual atmospheric mercury species in Downtown Toronto, Canada,
801 *J Environ Monitor*, 11, 660-669, Doi 10.1039/B815435j, 2009.

802 Spivakovsky, C. M., Logan, J. A., Montzka, S. A., Balkanski, Y. J., Foreman-Fowler, M., Jones, D. B.
803 A., Horowitz, L. W., Fusco, A. C., Brenninkmeijer, C. A. M., Prather, M. J., Wofsy, S. C., and McElroy,
804 M. B.: Three-dimensional climatological distribution of tropospheric OH: Update and evaluation, *J*
805 *Geophys Res-Atmos*, 105, 8931-8980, Doi 10.1029/1999jd901006, 2000.

806 Sprovieri, F., Pirrone, N., Landis, M. S., and Stevens, R. K.: Oxidation of gaseous elemental mercury to
807 gaseous divalent mercury during 2003 polar sunrise at Ny-Alesund, *Environmental Science &*
808 *Technology*, 39, 9156-9165, Doi 10.1021/Es050965o, 2005.

809 Sprovieri, F., Pirrone, N., Ebinghaus, R., Kock, H., and Dommergue, A.: A review of worldwide
810 atmospheric mercury measurements, *Atmos Chem Phys*, 10, 8245-8265, DOI
811 10.5194/acp-10-8245-2010, 2010.

812 Steffen, A., Douglas, T., Amyot, M., Ariya, P., Aspö, K., Berg, T., Bottenheim, J., Brooks, S., Cobbett,
813 F., Dastoor, A., Dommergue, A., Ebinghaus, R., Ferrari, C., Gardfeldt, K., Goodsite, M. E., Lean, D.,
814 Poulain, A. J., Scherz, C., Skov, H., Sommar, J., and Temme, C.: A synthesis of atmospheric mercury
815 depletion event chemistry in the atmosphere and snow, *Atmos Chem Phys*, 8, 1445-1482, 2008.

816 Steffen, A., Scherz, T., Olson, M., Gay, D., and Blanchard, P.: A comparison of data quality control
817 protocols for atmospheric mercury speciation measurements, *J Environ Monitor*, 14, 752-765,
818 10.1039/c2em10735j, 2012.

819 Stohl, A., Spichtinger-Rakowsky, N., Bonasoni, P., Feldmann, H., Memmesheimer, M., Scheel, H. E.,
820 Trickl, T., Hubener, S., Ringer, W., and Mandl, M.: The influence of stratospheric intrusions on alpine
821 ozone concentrations, *Atmos Environ*, 34, 1323-1354, Doi 10.1016/S1352-2310(99)00320-9, 2000.

822 Stohl, A., Forster, C., Frank, A., Seibert, P., and Wotawa, G.: Technical note: The Lagrangian particle
823 dispersion model FLEXPART version 6.2, *Atmos Chem Phys*, 5, 2461-2474, 2005.

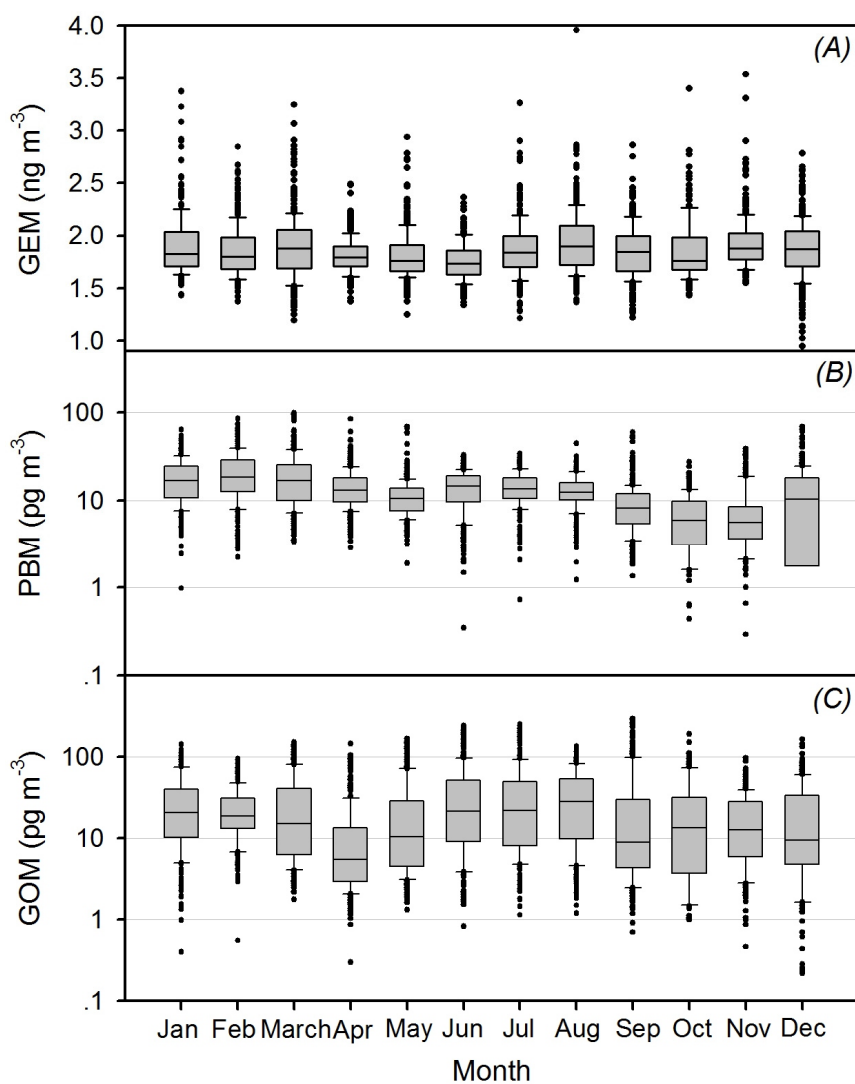
824 Subir, M., Ariya, P. A., and Dastoor, A. P.: A review of the sources of uncertainties in atmospheric
825 mercury modeling II. Mercury surface and heterogeneous chemistry - A missing link, *Atmos Environ*,
826 46, 1-10, DOI 10.1016/j.atmosenv.2011.07.047, 2012.

827 Swartzendruber, P. C., Jaffe, D. A., Prestbo, E. M., Weiss-Penzias, P., Selin, N. E., Park, R., Jacob, D. J.,
828 Strode, S., and Jaegle, L.: Observations of reactive gaseous mercury in the free troposphere at the
829 Mount Bachelor Observatory, *J Geophys Res-Atmos*, 111, Art. D24302
830 Doi 10.1029/2006jd007415, 2006.

831 Swartzendruber, P. C., Jaffe, D. A., and Finley, B.: Improved fluorescence peak integration in the
832 Tekran 2537 for applications with sub-optimal sample loadings, *Atmos Environ*, 43, 3648-3651,

833 10.1016/j.atmosenv.2009.02.063, 2009.
834 Talbot, R., Mao, H., Scheuer, E., Dibb, J., and Avery, M.: Total depletion of Hg degrees in the upper
835 troposphere-lower stratosphere, *Geophys Res Lett*, 34, Artn L23804
836 Doi 10.1029/2007gl031366, 2007.
837 Timonen, H., Ambrose, J. L., and Jaffe, D. A.: Oxidation of elemental Hg in anthropogenic and marine
838 airmasses, *Atmos. Chem. Phys.*, 13, 2827-2836, 10.5194/acp-13-2827-2013, 2013.
839 Tsamalis, C., Ravetta, F., Gheusi, F., Delbarre, H., and Augustin, P.: Mixing of free-tropospheric air
840 with the lowland boundary layer during anabatic transport to a high altitude station, *Atmos Res*, 143,
841 425-437, 10.1016/j.atmosres.2014.03.011, 2014.
842 Wang, F., Saiz-Lopez, A., Mahajan, A. S., Martin, J. C. G., Armstrong, D., Lemes, M., Hay, T., and
843 Prados-Roman, C.: Enhanced production of oxidised mercury over the tropical Pacific Ocean: a key
844 missing oxidation pathway, *Atmos Chem Phys*, 14, 1323-1335, 10.5194/acp-14-1323-2014, 2014.
845 Weiss-Penzias, P., Amos, H. M., Selin, N. E., Gustin, M. S., Jaffe, D. A., Obrist, D., Sheu, G. R., and
846 Giang, A.: Use of a global model to understand speciated atmospheric mercury observations at five
847 high-elevation sites (vol 15, pg 1161, 2015), *Atmos Chem Phys*, 15, 2225-2225, DOI
848 10.5194/acp-15-2225-2015, 2015.
849 Zeng, Y., and Hopke, P. K.: A Study of the Sources of Acid Precipitation in Ontario, Canada, *Atmos*
850 *Environ*, 23, 1499-1509, Doi 10.1016/0004-6981(89)90409-5, 1989.
851 Zhang, L. M., Wright, L. P., and Blanchard, P.: A review of current knowledge concerning dry
852 deposition of atmospheric mercury, *Atmos Environ*, 43, 5853-5864, DOI
853 10.1016/j.atmosenv.2009.08.019, 2009.
854
855
856
857
858
859
860
861
862
863
864

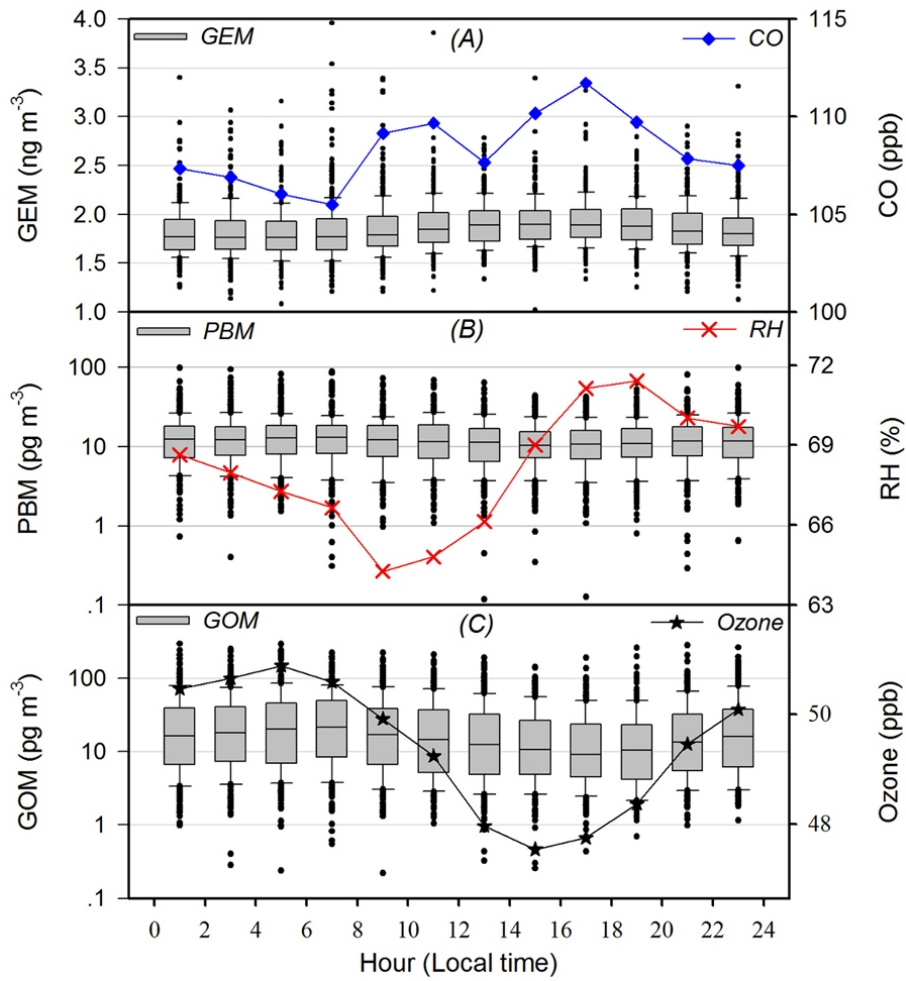
865 Figure 1. Monthly variation of atmospheric GEM (A), PBM (B), and GOM (C) at the PDM
866 Observatory. Box lines indicate the 10th, 25th, 50th, 75th, 90th percentiles, and data points
867 indicate concentrations below 10th and above 90th percentiles.



868

869

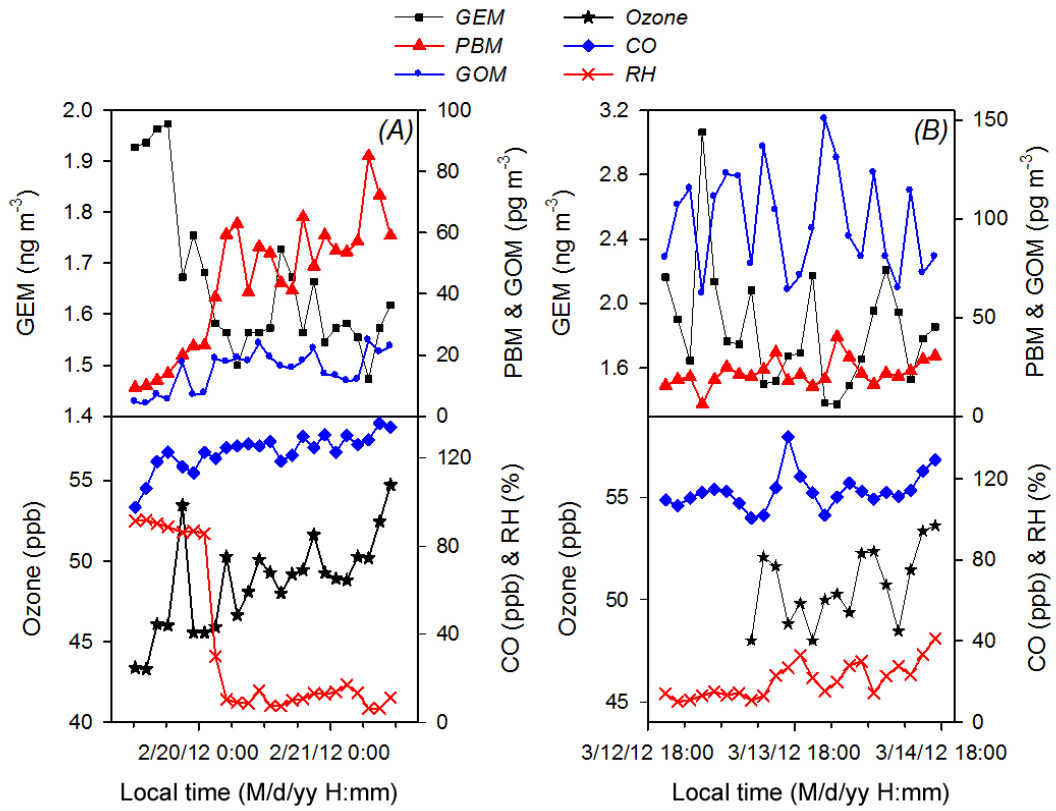
870 Figure 2. Diel, two-hour averaged, variations of atmospheric GEM and CO (A); PBM and relative
 871 humidity (RH) (B); and GOM and ozone (C) at the PDM Observatory. Box lines indicate
 872 the 10th, 25th, 50th, 75th, 90th percentiles, and data points indicate concentrations below 10th
 873 and above 90th percentiles.



874
 875

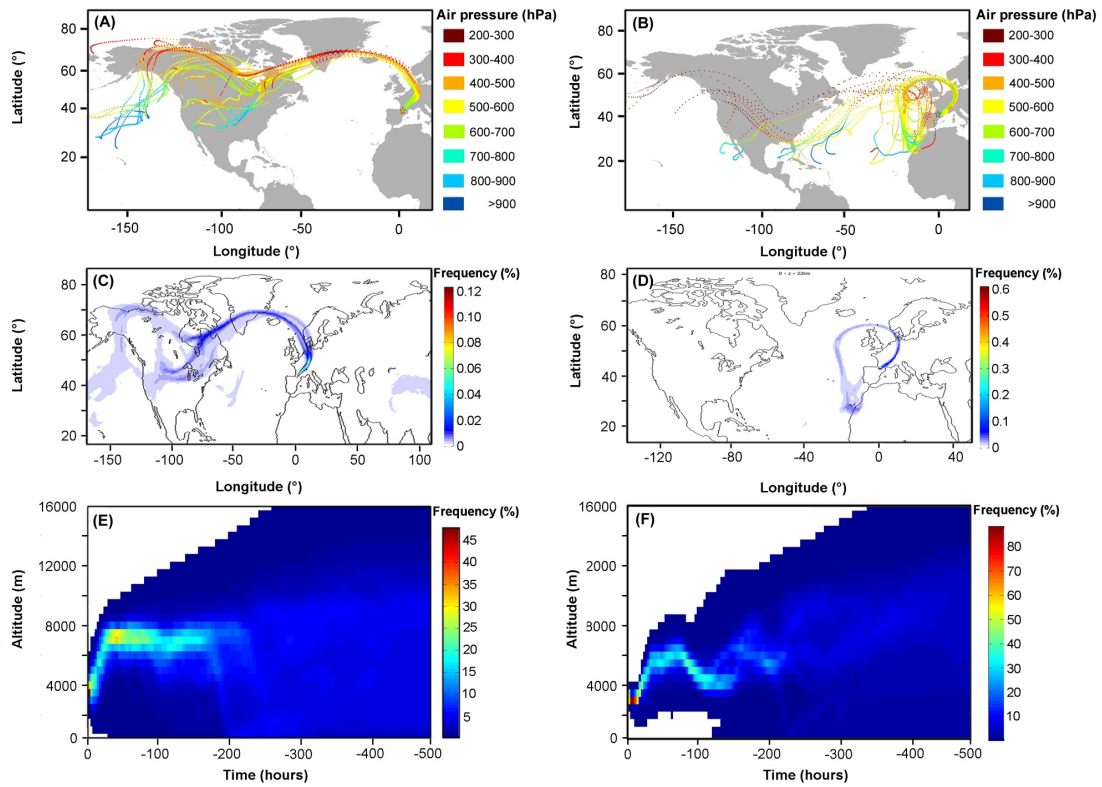
876
877
878

Figure 3. Time series of GEM, PBM, GOM, ozone, CO, and relative humidity (RH) during high PBM event #12 (A) and #19 (B).



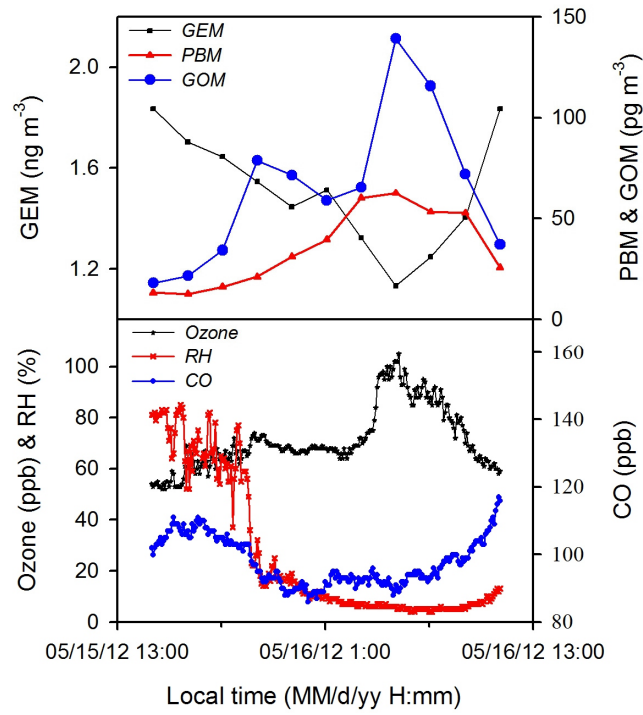
879
880

881 Figure 4. 240-h Hysplit air mass backward trajectories for the typical high PBM events #12 (A)
882 and #19 (B), Flexpart simulated air mass source regions of high PBM events #12 (C) and #19
883 (D) and Flexpart simulated air mass travelling heights of PBM events #12 (E) and #19 (F). To
884 reduce the uncertainty related to Hysplit trajectory simulations (Gustin et al., 2012), Hysplit
885 trajectories were calculated for each of the events ended at 27 locations evenly-distributed in
886 a $0.5^\circ \times 0.5^\circ$ grid cell and at a height of -500 m, 0 m, and 500 m around the PDM Observatory.



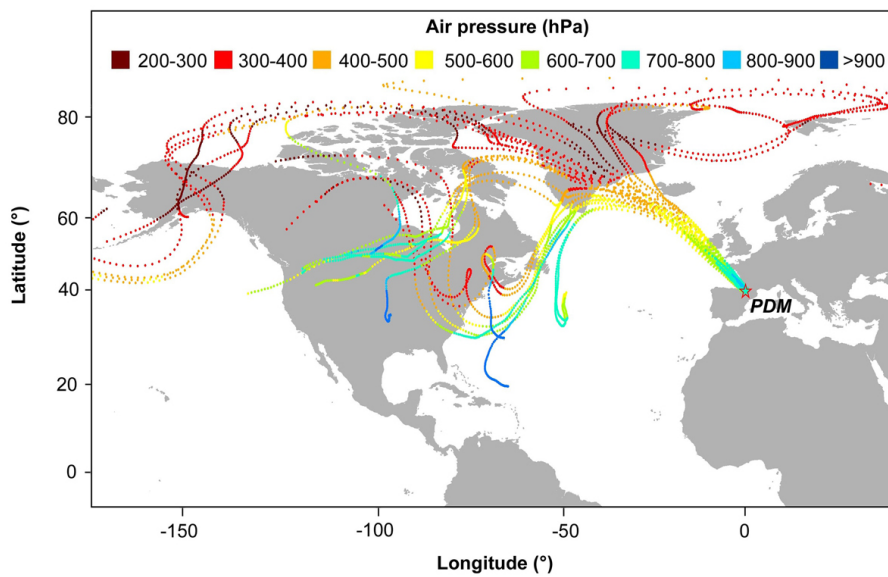
887
888

889 Figure 5. Time series of GEM, PBM, GOM, ozone, CO, and relative humidity (RH) during high
890 GOM event #7.



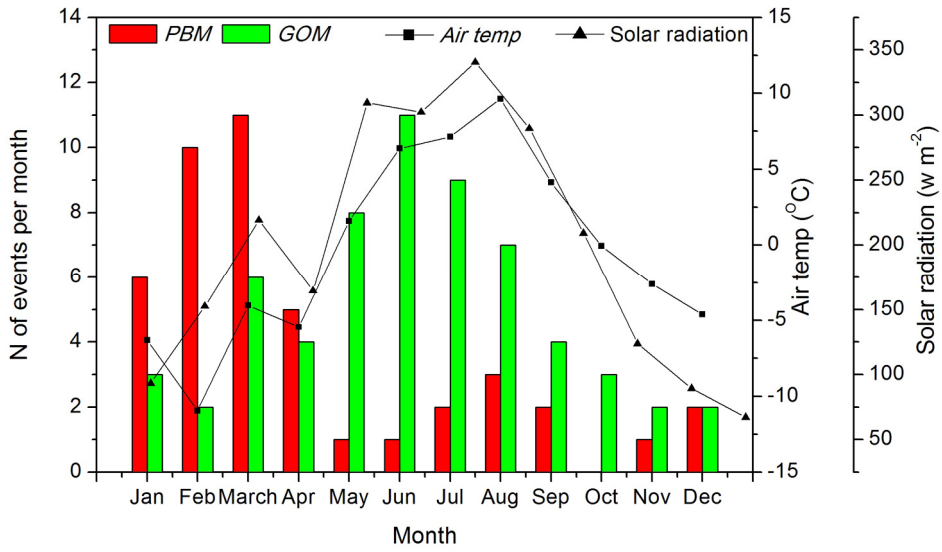
891
892
893
894

895 Figure 6. 168-h Hysplit air mass backward trajectories for the typical high GOM event #7. To
896 reduce the uncertainty related to trajectory simulations (Gustin et al., 2012), trajectories were
897 calculated for 27 locations evenly-distributed in a $0.5^\circ \times 0.5^\circ$ grid cell and at a height of -500
898 m, 0 m, and 500 m around the PDM Observatory.



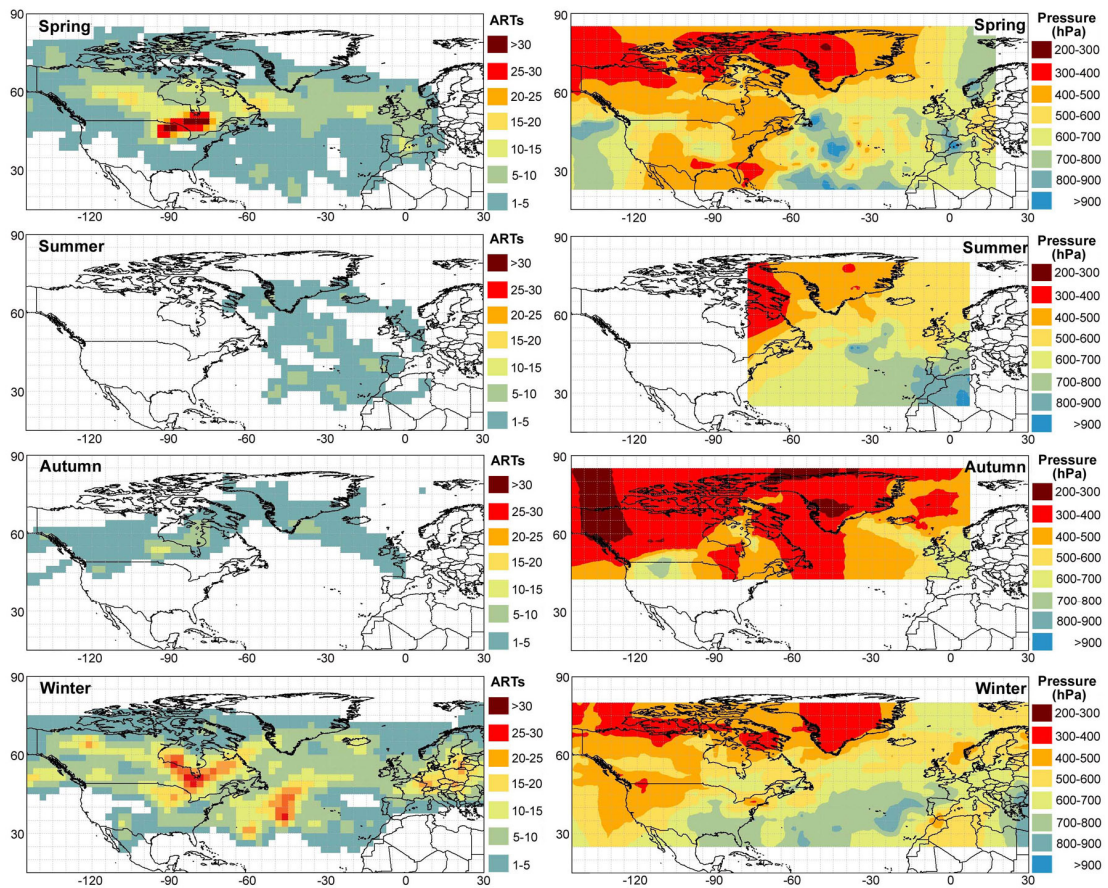
899
900
901
902

903 Figure 7. Monthly variations in the frequency of high PBM and GOM events at the PDM
904 Observatory.



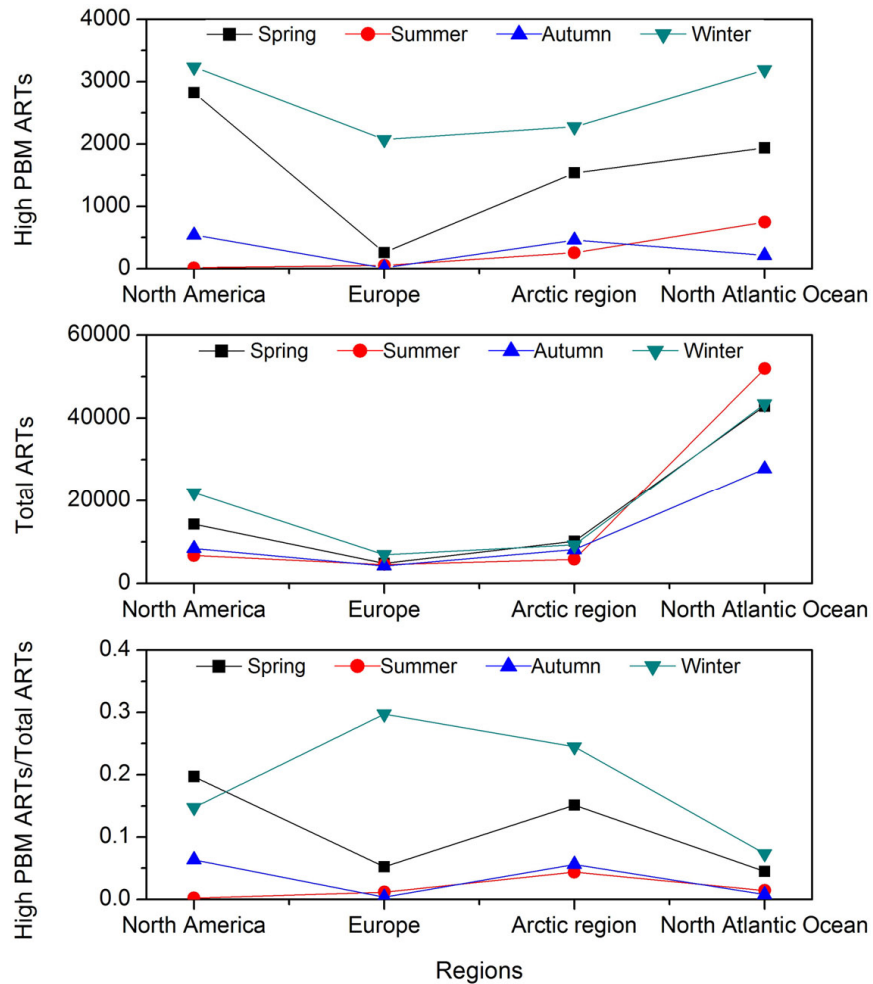
905
906
907
908
909

910 Figure 8. Air mass residence times (ARTs) and averaged pressure of air masses associated with
911 high PBM events for each season during the study period.



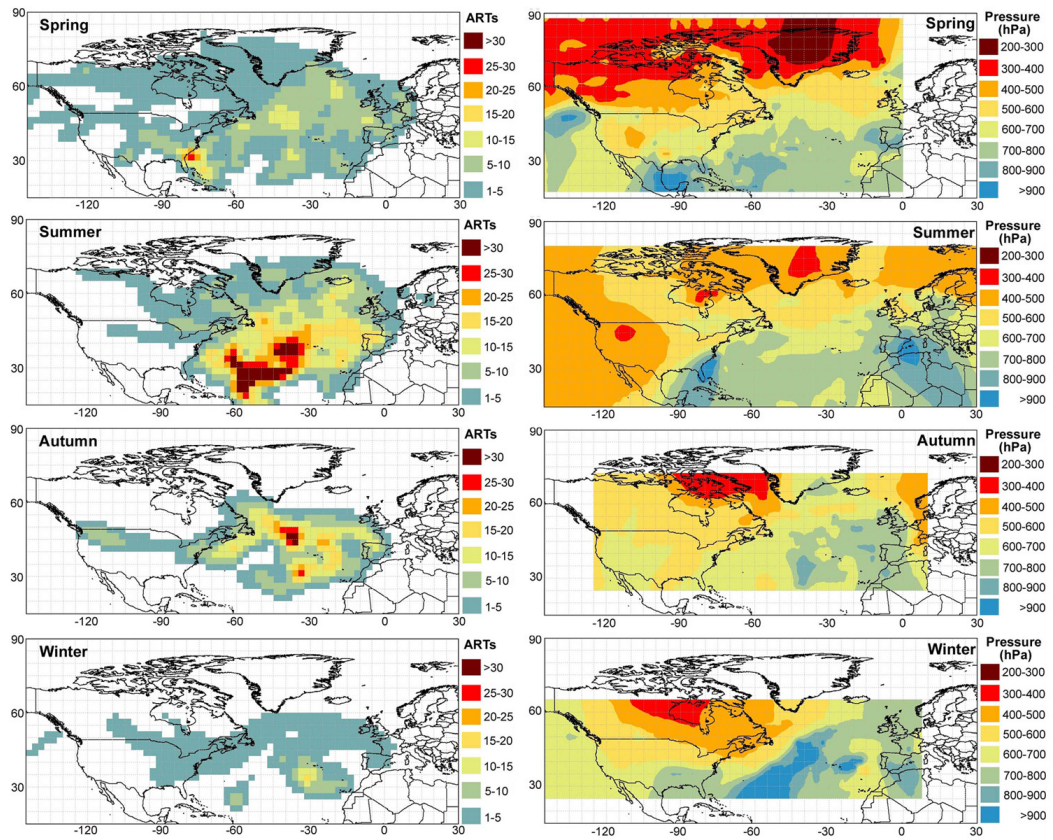
912
913
914

915 Figure 9. Seasonal variations in air masses residence times associated with high PBM events (high
 916 PBM ARTs, top), total residence times of all the air masses (Total ARTs, middle) and high
 917 PBM ARTs/Total ARTs ratios (bottom) in the North America, Europe, Arctic region and
 918 North Atlantic Ocean.



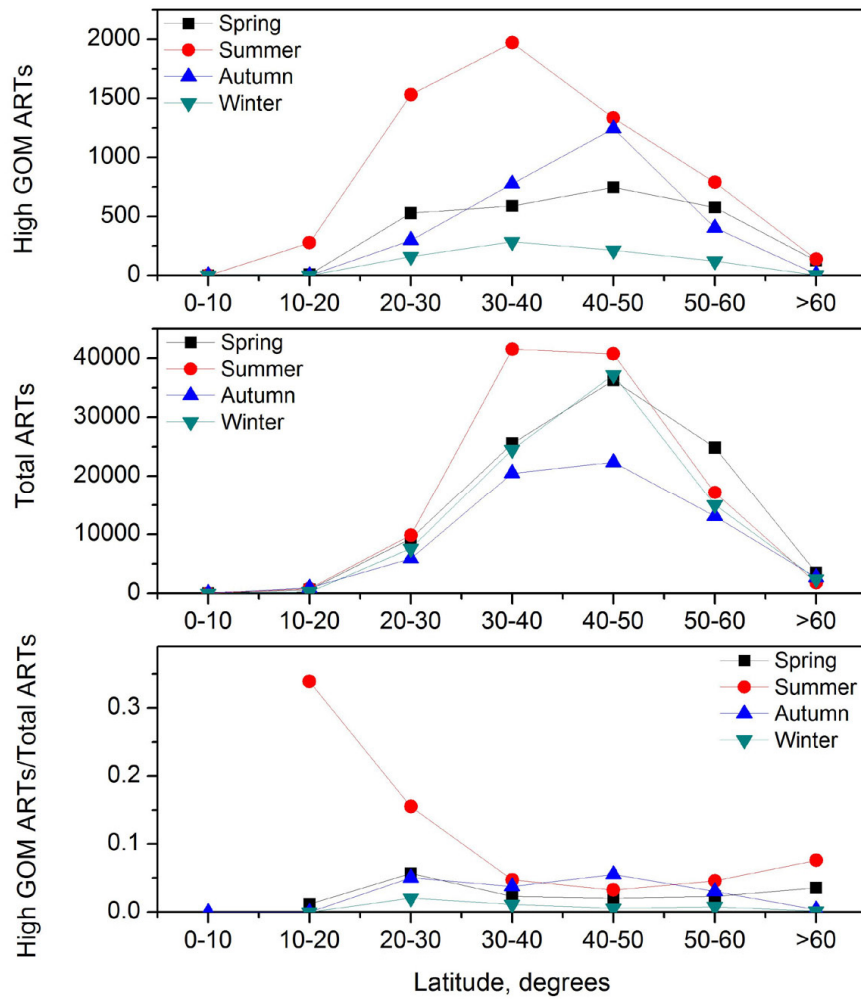
919
 920
 921
 922
 923
 924
 925
 926
 927
 928
 929
 930
 931
 932
 933
 934

935 Figure 10. Air mass residence times (ARTs) and averaged pressure of air masses associated with
936 high GOM events for each season during the study period.



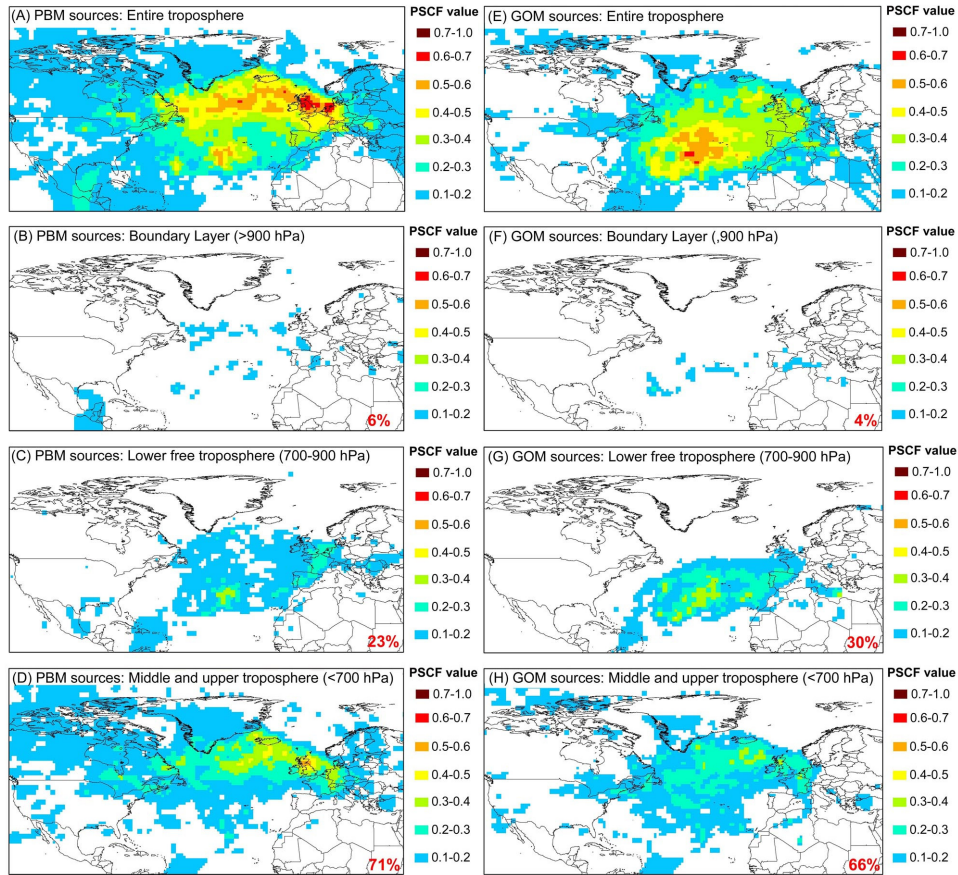
937
938
939
940

941 Figure 11. Latitude dependence of Air masses residence times (ARTs, top) associated with high
 942 GOM events, total residence times of all the air masses (Total ARTs, middle) and high GOM
 943 ARTs/Total ARTs ratios (bottom) over the North Atlantic Ocean for each season.



944
 945
 946
 947

948 Figure 12. Map showing the identified potential source regions of PBM during the whole study
 949 period for (A) entire troposphere, (B) boundary layer, (C) lower free troposphere, and (D)
 950 middle and upper troposphere and potential source regions of GOM for (E) entire troposphere,
 951 (F) boundary layer, (G) lower free troposphere, and (G) middle and upper
 952 troposphere.



953